The Carina project. IX. on hydrogen and helium burning variables

Coppola, G.; Marconi, M.; Stetson, P. B.; Bono, G.; Braga, V. F.; Ripepi, V.; Dall'ora, M.; Musella, I.; Buonanno, R.; Fabrizio, M.; Ferraro, I.; Fiorentino, G.; Iannicola, G.; Monelli, M.; Nonino, M.; Thévenin, F.; Walker, A. R.

Publisher's version / Version de l'éditeur:
https://doi.org/10.1088/0004-637X/814/1/71
The Astrophysical Journal, 814, 71, 2015-11-17

The Astrophysical Journal, 814:71 (28pp), 2015 November 20 doi:10.1088/0004-637X/814/1/71

THE CARINA PROJECT. IX. ON HYDROGEN AND HELIUM BURNING VARIABLES

G. Coppola[1], M. Marconi[1], P. B. Stetson[2], G. Bono[3,4], V. F. Braga[3,4], V. Ripepi[1], M. Dall'Ora[1], I. Musella[1], R. Buonanno[3,5], M. Fabrizio[5], I. Ferraro[4], G. Fiorentino[6], G. Iannicola[4], M. Monelli[7,8], M. Nonino[9], F. Thévenin[10], and A. R. Walker[11]

[1] INAF—Osservatorio Astronomico di Capodimonte, Via Moiariello 16, I-80131 Napoli, Italy; marcella@oacn.inaf.it
[2] National Research Council, 5071 West Saanich Road, Victoria, BC V9E 2E7, Canada
[3] Dipartimento di Fisica, Universitá di Roma Tor Vergata, Via della Ricerca Scientifica 1, I-00133 Roma, Italy
[4] INAF—Osservatorio Astronomico di Roma, Via Frascati 33, I-00040 Monte Porzio Catone, Italy
[5] INAF—Osservatorio Astronomico di Teramo, via M. Maggini, I-64110, Teramo, Italy
[6] INAF—Osservatorio Astronomico di Bologna, via Ranzani 1, I-40127, Bologna, Italy
[7] Instituto de Astrofísica de Canarias, Calle Via Lactea s/n, E-38205 La Laguna, Tenerife, Spain
[8] Departmento de Astrofísica, Universidad de La Laguna, E-38200 La Laguna, Tenerife, Spain
[9] INAF—Osservatorio Astronomico di Trieste, via G. B. Tiepolo 11, I-40131 Trieste, Italy
[10] Laboratoire Lagrange, Universit Cte d'Azur, Observatoire de la Cte d'Azur, CNRS, Blvd de l'Observatoire, CS 34229, F-06304 Nice cedex 4, France
[11] Cerro Tololo Inter-American Observatory, National Optical Astronomy Observatory, Casilla 603, La Serena, Chile

Received 2015 July 7; accepted 2015 September 8; published 2015 November 17

ABSTRACT

We present new multiband (*UBVI*) time-series data of helium burning variables in the Carina dwarf spheroidal galaxy. The current sample includes 92 RR Lyrae—six of them are new identifications—and 20 Anomalous Cepheids, one of which is new identification. The analysis of the Bailey diagram shows that the luminosity amplitude of the first overtone component in double-mode variables is located along the long-period tail of regular first overtone variables, while the fundamental component is located along the short-period tail of regular fundamental variables. This evidence further supports the transitional nature of these objects. Moreover, the distribution of Carina double-mode variables in the Petersen diagram (P_1/P_0 versus P_0) is similar to metal-poor globulars (M15, M68), to the dwarf spheroidal Draco, and to the Galactic Halo. This suggests that the Carina old stellar population is metal-poor and affected by a small spread in metallicity. We use trigonometric parallaxes for five field RR Lyrae stars to provide an independent estimate of the Carina distance using the observed reddening free Period–Wesenheit [PW, (*BV*)] relation. Theory and observations indicate that this diagnostic is independent of metallicity. We found a true distance modulus of $\mu = 20.01 \pm 0.02$ (standard error of the mean) $\pm$ 0.05 (standard deviation) mag. We also provided independent estimates of the Carina true distance modulus using four predicted PW relations (*BV, BI, VI, BVI*) and we found: $\mu = (20.08 \pm 0.007 \pm 0.07)$ mag, $\mu = (20.06 \pm 0.006 \pm 0.06)$ mag, $\mu = (20.07 \pm 0.008 \pm 0.08)$ mag, and $\mu = (20.06 \pm 0.006 \pm 0.06)$ mag. Finally, we identified more than 100 new SX Phoenicis stars that together with those already known in the literature (340) make Carina a fundamental laboratory for constraining the evolutionary and pulsation properties of these transitional variables.

Key words: galaxies: individual (Carina) – Local Group – stars: distances – stars: oscillations (including pulsations) – stars: variables: RR Lyrae

Supporting material: figure set, machine-readable tables

1. INTRODUCTION

Dwarf galaxies play a crucial role in several astrophysical and cosmological problems. They outnumber giant stellar systems in the nearby universe and at low redshift (see, e.g., Mateo et al. 1998; McConnachie 2012), but it seems that the number is steadily decreasing at large redshifts (Baldry et al. 2012; Mortlock et al. 2013). The current empirical evidence indicates that the luminosity function does not peak at low-surface brightness systems at redshifts larger than $z = 2$ (Bauer et al. 2011; Weinzirl et al. 2011). It is clear that in this context the age distribution of the old stellar populations in nearby dwarf galaxies plays a crucial role in constraining their early formation and evolution (Salvadori et al. 2010). Current empirical evidence indicates that both early- and late-type dwarf galaxies host stellar populations older than 10 Gyr. This evidence applies not only to IC10, the Local Group prototype of star-forming galaxies (Sanna et al. 2009), but also to the recently discovered Ultra Faint Dwarf galaxies (Dall'Ora et al. 2006, 2012; Greco et al. 2008; Kuehn et al. 2008; Moretti et al. 2009; Musella et al. 2009, 2012; Clementini et al. 2012; Garofalo et al. 2013; Fabrizio et al. 2014). Moreover, the comparison between old stellar populations in nearby dwarfs and Galactic Globular clusters does not show, at fixed metal content, any striking difference concerning the age distribution (Monelli et al. 2003; Cole et al. 2007; Bono et al. 2010).

The above empirical evidence suggests that low-mass dark matter halos started assembling baryons at about the same time as the giant halos (Springel et al. 2005; Bauer et al. 2011; Duncan et al. 2014). Detailed constraints on the formation of these systems require detailed investigations into their star-formation histories. However, this approach needs deep and accurate color–magnitude diagrams (CMDs) down to limiting magnitudes fainter than the main-sequence turnoff of the old stellar populations (Gallart et al. 2005; Monelli et al. 2010b). In this context variable stars play a crucial role, since they can be easily identified. Moreover, they cover a broad range in age, from a few 100 Myr for Classical Cepheids (e.g., Bono et al. 2005) to a few Gyr for Anomalous Cepheids (AC) (e.g., Caputo 1998; Marconi et al. 2004) to ages older than 10 Gyr for the RR Lyrae stars (RRLs; e.g., Castellani et al. 1991).

Table 1
Log of Observations

	Run ID	Dates	Telescope	Camera	U	B	V	R	I	Multiplex
1	susi9810:	1998 Oct 26–29	ESO NTT 3.6 m	SUSI	…	…	2	…	3	×2
2	wfi38:	1999 Oct 30–11 14	MPI/ESO 2.2 m	WFI	…	3	…	2	…	×8
3	susi0410:	2004 Oct 05–09	ESO NTT 3.6 m	SUSI	…	…	…	12	…	×2
4	B05jan12:	2005 Jan 12	CTIO 4.0 m	Mosaic2	12	…	…	…	5	×8
5	B05jan17:	2005 Jan 18	CTIO 4.0 m	Mosaic2	…	2	6	…	21	×8
6	B0512:	2005 Dec 28	CTIO 4.0 m	Mosaic2	14	…	2	…	1	×8
7	B0712:	2007 Dec 14–19	CTIO 4.0 m	Mosaic2	…	71	88	…	…	×8
8	B1002:	2010 Jan 14–16	CTIO 4 m	Mosaic2	…	…	19	…	…	×8
9	wfi41:	2012 Feb 22–29	MPI/ESO 2.2 m	WFI	6	3	…	…	3	×8

However, for classical Cepheids we have evidence of tight correlation between pulsation and evolutionary age (Matsunaga et al. 2011, 2013). The same outcome does not apply, as noted by the referee, to the other quoted variables. This means that for RRLs we can only provide a lower limit to their individual ages (Bono et al. 2011), while for ACs we can only provide an age interval.

The latter two groups have several distinctive features that make them solid stellar tracers in resolved dwarf spheroidal galaxies. Empirical evidence indicates that all the dSphs that have been searched for evolved helium burning variable stars host RRLs. It is worth mentioning that they have been identified in all stellar systems hosting a stellar population older than 10 Gyr and an intermediate horizontal branch (HB) morphology, i.e., systems in which the mass distribution along the HB covers the RRL instability strip (IS). The stellar systems with ages younger than 10 Gyr typically display Galactic thin disk kinematics (Blanco-Cuaresma et al. 2015). This means that we still lack solid empirical evidence of RR Lyrae belonging to old thin disk open clusters (Bono et al. 2011). On the other hand, ACs have been identified in stellar systems more metal-poor than about [Fe/H] = −1.6 dex. Theoretical predictions indicate that helium burning sequence of intermediate-mass stars more metal-rich than the above limit do not cross the so-called Cepheid IS (Castellani & degl'Innocenti 1995; Stetson et al. 2014b).

It goes without saying that the comparison of pulsation and evolutionary properties of evolved helium burning-variables in nearby stellar systems allows us to constrain their early formation (Fiorentino et al. 2012, 2015a; Coppola et al. 2013; Stetson et al. 2014b). The Carina dSph is a very interesting laboratory for investigating the above issues. In a previous investigation we compared the period distribution of the central helium burning variable stars in Carina with similar distributions in nearby dSphs and in the Large Magellanic Cloud (LMC) and we found that the old stellar populations in these systems share similar properties (Coppola et al. 2013, hereafter, Paper VI). On the other hand, the period distribution and the Bailey diagram (luminosity amplitude versus period) of ACs show significant differences among the above stellar systems. This evidence suggested that the properties of intermediate-age stellar populations might be affected both by environmental effects and structural parameters.

In this investigation we move toward a complete census of helium-burning variable stars. The structure of the paper is the following. In Section 2 we present in detail the adopted photometric data set together with the light curves of both RRLs and ACs and their pulsation properties. In Section 3 we discuss the properties of RRLs and ACs using the Bailey diagram and the Petersen diagram (period ratio versus period). We focused our attention on the position of double mode variables and on the sensitivity of the period ratio on the iron abundance. In Section 4 we use the optical Period–Wesenheit–Metallicity (PWZ) relation of RRLs to estimate the Carina true distance modulus. To constrain the possible occurrence of systematic errors we estimated the Carina distance using the five field RRLs for which accurate estimates of their trigonometric parallaxes are available. Independent distance determinations were also provided using predicted optical PWZ relations. In Section 5 we present preliminary results about SX Phoenicis variables. Finally, in Section 6 we summarize the results of this investigation and briefly outline the future development of the Carina project.

2. PHOTOMETRIC DATA

The photometric catalog adopted in this investigation is an extension of the data set discussed by Coppola et al. (2013). This included 4474 CCD images in the *UBVRI* photometric bands obtained with the CTIO 4 m and 1.5 m telescopes, the ESO 3.6 m NTT, the MPI/ESO 2.2 m telescope, and the 8 m ESO VLT during the period 1992 December through 2008 September. Here we add 2028 CCD images in the same photometric bands obtained with the same telescopes (see Table 1). In the current analysis, the *R*-band data were not included because the number of measurements is limited and they do not provide a good coverage of the pulsation cycle. The seeing had a median value of 1$''$.0, and ranged from 0$''$.8 (10-percentile) and 0$''$.9 (25-percentile) to 1$''$.3 (75-percentile) and 1$''$.6 (90-percentile). The reader interested in a detailed discussion of the photometric methodology, the absolute photometric calibration, the identification of the variable stars and analysis of the time series data is referred to Paper VI and to Stetson et al. (2014b).

The list of variable stars begins with that from Dall'Ora et al. (2003, hereafter D03), who merged the prior lists of Saha et al. (1986, hereafter S86), and performed their own comprehensive investigation of the resulting set of 92 candidate variable stars. This existing star list has been augmented by our own search for new variables within the new, expanded set of 6992 optical images of Carina. In particular, we have identified 92 RRLs. Among them 12 pulsate in the first-overtone (FO, RR_c), 63 in the fundamental mode (F, RR_{ab}), 9 are double-mode pulsators (RR_d) and 8 are candidate Blazhko variables (Bl). We also identified 20 ACs, 2 long-period variables (LPV) and 10 geometrical variables (eclipsing binaries, EB, and W Uma). The main difference between the current set of variable stars and those discussed in Paper VI is that we have identified 16 new variables. Among them are six RRLs, one AC, seven EBs

Table 2
Catalog of Carina Variable Stars

ID	α (J2000.0)	δ (J2000.0)	S86	D03	VM13	Paper VI	Our
…	(hh mm ss)	(dd mm ss)	…	…	…	…	…
V3	06 43 31.71	−50 51 05.3	ab	…	…	V215 (ab)	ab
V4	06 43 28.70	−50 55 46.9	c	V177 (c)	…	…	c
V7	06 43 16.26	−51 04 17.2	ab	V7 (ab)	…	V7 (ab)	ab
V10	06 43 10.66	−50 43 47.8	ab	V10 (ab)	…	V10 (ab)	ab
V11	06 43 08.20	−50 50 47.9	c	V11 (d)	…	V11 (d)	d
V14	06 43 01.93	−51 01 26.3	ab	V14 (AC)	…	V14 (AC)	AC
V22	06 42 46.32	−50 57 36.9	ab	V22 (c)	…	V22 (ab)	ab
V24	06 42 34.00	−50 44 24.9	ab	V24 (ab)	…	V24 (ab)	ab
V25	06 42 32.22	−50 59 36.4	ab	…	…	V213 (ab)	Bl
V26	06 42 30.33	−50 52 24.1	ab	V26 (d)	…	V26 (d)	d
V27	06 42 28.89	−50 47 50.2	ab	V27 (AC)	…	V27 (AC)	AC
V29	06 42 25.07	−51 03 47.7	ab	V29 (AC)	…	V29 (AC)	AC
V30	06 42 24.10	−51 02 38.9	ab	V30 (ab)	…	V30 (ab)	ab
V31	06 42 22.87	−50 59 16.0	c	V31 (ab)	…	V31 (ab)	Bl
V32	06 42 22.50	−50 59 18.3	ab	V202 (ab)	…	V202 (ab)	ab
V33	06 42 21.10	−51 11 51.4	ab	V33 (AC)	…	V33 (AC)	AC
V34	06 42 19.22	−50 45 30.7	ab	V34 (ab)	…	V34 (ab)	ab
V40	06 42 15.63	−51 07 00.0	c (ab?)	V40 (c)	…	V40 (c)	c
V41	06 42 14.76	−50 55 14.0	SV	V180 (AC)	…	V180 (AC)	AC
V43	06 42 13.11	−50 46 49.9	c	V43 (c)	…	V43 (c)	c
V44	06 42 13.05	−50 57 22.1	ab	…	…	V212 (ab)	ab
V47	06 42 09.10	−50 53 53.5	c	V47 (c)	37 (ab)	V47 (c)	c
V49	06 42 08.77	−51 01 11.8	ab	V49 (ab)	…	V49 (ab)	ab
V57	06 42 02.85	−50 52 56.8	ab	V57 (ab)	35 (ab)	V57 (ab)	ab
V58	06 42 01.04	−50 57 19.7	ab	…	34 (ab)	V211 (ab)	ab
V60	06 41 59.75	−51 06 38.5	ab	V60 (ab)	33 (ab)	V60 (ab)	ab
V61	06 41 58.29	−50 47 37.8	ab	V61 (ab)	32 (ab)	V61 (ab)	Bl
V65	06 41 55.86	−50 55 35.3	ab	V65 (ab)	31 (ab)	V65 (ab)	ab
V67	06 41 52.64	−51 05 19.7	ab	V67 (ab)	30 (ab)	V67 (ab)	ab
V68	06 41 49.15	−50 59 18.7	ab	V68 (ab)	28 (ab)	V68 (ab)	ab
V73	06 41 46.91	−51 07 07.5	ab	V73 (ab)	27 (ab)	V73 (ab)	ab
V74	06 41 43.86	−50 54 09.0	c	V74 (c)	…	V74 (c)	d
V75	06 41 42.90	−50 58 49.5	ab	…	25 (ab)	…	ab
V77	06 41 39.24	−51 05 39.7	ab	V77 (ab)	23 (ab)	V77 (Bl)	Bl
V84	06 41 37.11	−51 00 04.5	ab	V84 (ab)	…	V84 (ab)	ab
V85	06 41 35.64	−50 50 07.4	ab	V85 (ab)	22 (ab)	V85 (ab)	ab
V87	06 41 32.67	−50 57 00.8	SV	V87 (AC)	3 (AC)	V87 (AC)	AC
V89	06 41 29.94	−50 47 13.7	ab	V89 (d)	21 (ab)	V89 (d)	d
V90	06 41 29.92	−50 52 10.7	ab	V90(ab)	20 (ab)	V90 (ab)	ab
V91	06 41 29.46	−51 04 28.5	ab	V91 (ab)	19 (ab)	V91 (ab)	ab
V92	06 41 28.75	−51 06 50.5	ab	V92 (ab)	18 (ab)	V92 (ab)	ab
V105	06 41 16.53	−51 09 03.0	ab	V105 (ab)	14 (ab)	V105 (ab)	ab
V115	06 41 06.23	−50 53 18.5	?	V115 (AC)	…	V115 (AC)	AC
V116	06 41 05.63	−51 00 28.1	ab	V116 (ab)	11 (ab)	V116 (ab)	ab
V122	06 40 56.97	−51 00 45.8	ab	V122(ab)	…	V122 (ab)	ab
V123	06 40 54.92	−50 44 14.5	ab	V123 (ab)	…	V123 (ab)	ab
V124	06 40 53.78	−51 05 53.1	ab	V124 (ab)	…	V124 (ab)	ab
V125	06 40 53.37	−50 58 53.3	ab	V125 (ab)	10 (c)	V125 (ab)	ab
V126	06 40 52.35	−50 58 56.6	ab	V126 (ab)	…	V126 (Bl)	Bl
V127	06 40 52.22	−50 59 20.8	ab	V127 (ab)	…	V127 (Bl)	Bl
V129	06 40 49.34	−51 08 15.0	ab	V129 (AC)	…	V129 (AC)	AC
V133	06 40 47.93	−51 03 23.5	ab	…	…	V209 (ab)	ab
V135	06 40 46.43	−51 05 24.6	ab	V135 (ab)	…	V135 (ab)	ab
V136	06 40 44.80	−51 12 42.7	ab	V136 (ab)	…	V136 (ab)	ab
V138	06 40 40.73	−50 52 58.3	SV	V138 (ab)	…	V138 (ab)	ab
V141	06 40 39.29	−50 56 01.3	SV	V141 (ab)	…	V141 (ab)	ab
V142	06 40 38.40	−51 01 38.8	SV	V142 (c)	…	V142 (c)	c
V143	06 40 38.06	−51 11 30.9	ab	V143 (ab)	…	V143 (ab)	ab
V144	06 40 37.20	−50 59 25.0	c	V144 (c)	9 (c)	V144 (c)	c
V148	06 40 31.69	−50 48 39.9	ab	V148(c)	8 (c)	V148 (c)	c
V149	06 40 30.46	−51 07 00.9	ab	V149 (AC)	…	V149 (AC)	AC

Table 2
(Continued)

ID	α (J2000.0)	δ (J2000.0)	S86	D03	VM13	Paper VI	Our
…	(hh mm ss)	(dd mm ss)	…	…	…	…	…
V151	06 40 29.45	−51 00 17.3	SV	V151 (c)	7 (c)	V151 (c)	c
V153	06 40 24.39	−51 04 49.9	ab	V153 (ab)	…	V153 (ab)	ab
V158	06 40 12.87	−50 56 24.8	ab	V158 (ab)	…	V158 (ab)	ab
V159	06 40 12.59	−51 09 35.8	ab	V159 (ab)	…	V159 (ab)	ab
V164	06 39 56.29	−50 53 54.7	ab	V164 (ab)	…	V164 (ab)	ab
V165	06 39 55.72	−50 59 49.2	ab	V186 (ab)	…	V186 (ab)	ab
V170	06 39 38.54	−50 46 33.6	ab	…	…	…	ab
V171	06 39 36.54	−51 12 40.7	ab	…	…	…	ab
V173	06 43 27.13	−50 44 49.2	…	V173 (RGB)	…	V173 (RGB)	RGB
V174	06 42 38.13	−50 46 10.9	…	V174 (ab)	…	V174 (ab)	ab
V175	06 42 54.36	−50 51 21.6	…	V175 (c)	...	V175 (c)	c
V176	06 43 00.06	−50 53 59.1	…	V176 (c)	…	V176 (ab)	ab
V178	06 41 44.04	−50 50 17.2	…	V178 (AC)	5 (AC)	V178 (AC)	AC
V179	06 41 49.40	−50 54 11.2	…	V179 (ab)	29 (c)	V179 (ab)	ab
V181	06 42 24.16	−50 56 00.3	…	V181 (c)	…	V181 (c)	c
V182	06 41 34.93	−50 52 39.1	…	V182 (ab)	…	V182 (ab)	ab
V183	06 41 27.59	−50 56 01.4	…	V183 (ab)	17 (ab)	V183 (ab)	ab
V184	06 40 33.02	−50 43 14.8	…	V184 (c)	…	V184 (c)	c
V185	06 40 25.22	−50 44 35.4	…	V185 (ab)	…	V185 (ab)	ab
V187	06 40 24.74	−51 01 29.4	…	V187 (AC)	…	V187 (AC)	AC
V188	06 40 12.28	−51 07 06.2	…	V188 (ab)	…	V188 (ab)	ab
V189	06 40 09.85	−51 08 05.2	…	V189 (ab)	6 (c)	V189 (ab)	ab
V190	06 41 39.78	−50 59 02.1	…	V190 (AC)	4 (AC)	V190 (AC)	AC
V191	06 41 26.22	−50 59 33.9	…	V191 (ab)	16 (ab)	V191 (ab)	ab
V192	06 41 20.66	−51 00 31.5	…	V192 (d)	15 (ab)	V192 (d)	d
V193	06 41 28.23	−51 00 45.4	…	V193 (AC)	2 (AC)	V193 (AC)	AC
V194	06 41 04.23	−51 01 32.9	…	V194 (FV)	…	V194 (FV)	FV
V195	06 41 40.82	−51 01 33.7	…	V195 (ab)	24 (ab)	V195 (ab)	ab
V196	06 41 11.48	−51 02 16.1	…	V196 (ab)	13 (ab)	V196 (ab)	ab
V197	06 41 00.27	−51 02 39.5	…	V197 (c)	…	V197 (c)	c
V198	06 41 10.55	−51 03 22.9	…	V198 (d)	12 (c)	V198 (d)	d
V199	06 41 19.60	−51 10 23.7	…	V199 (ab)	…	V199 (ab)	ab
V200	06 41 46.74	−50 58 39.3	…	V200 (ab)	26 (ab)	V200 (ab)	ab
V201	06 42 10.38	−50 59 07.5	…	V201 (ab)	…	V201 (ab)	ab
V203	06 41 56.12	−50 59 21.6	…	V203 (AC)	6 (AC)	V203 (AC)	AC
V204	06 42 04.10	−51 01 51.4	…	V204 (ab)	…	V204 (ab)	ab
V205	06 42 24.51	−51 02 40.4	…	V205 (AC)	7 (AC)	V205 (AC)	AC
V206	06 42 04.25	−51 09 41.3	…	V206 (ab)	36 (ab)	V206 (ab)	Bl
V207	06 43 07.50	−51 02 30.9	…	V207 (d)	…	V207 (d)	d
V208*	06 40 22.40	−51 17 08.1	…	…	…	V208 (ab)	ab
V210*	06 41 27.04	−51 15 39.8	…	…	…	V210(Bl)	d
V214*	06 42 36.99	−51 03 29.7	…	…	…	V214 (Bl)	Bl
V216*	06 41 17.76	−50 56 46.0	…	…	…	V216 (AC)	AC
V217*	06 41 33.03	−50 47 56.0	…	…	…	V217 (AC)	AC
V218*	06 41 39.56	−51 15 52.6	…	…	…	V218 (AC)	AC
V219*	06 42 09.01	−50 59 37.6	…	…	…	V219 (AC)	AC
V220*	06 40 19.12	−50 58 23.0	…	…	…	V220 (EB)	EB
V221*	06 43 20.73	−50 55 29.9	…	…	…	V221 (WUma)	WUma
V222*	06 41 24.30	−51 03 24.7	…	…	…	…	LPV
V223*	06 39 52.92	−50 54 28.3	…	…	…	…	ab
V224*	06 40 36.37	−51 16 42.2	…	…	…	…	LPV
V225*	06 41 01.01	−51 00 02.4	…	…	…	…	d
V226*	06 40 18.76	−51 18 36.6	…	…	…	…	ab
V227*	06 41 26.13	−51 21 26.7	…	…	…	…	ab
V228*	06 42 35.07	−50 38 07.2	…	…	…	…	ab
V229*	06 39 38.92	−51 05 59.1	…	…	…	…	ab
V230*	06 42 34.11	−50 58 20.0	…	…	8 (AC)	…	AC
V231*	06 41 10.58	−50 53 40.1	…	…	…	…	EB
V232*	06 40 10.11	−51 16 01.5	…	…	…	…	EB
V233*	06 41 23.47	−50 54 03.0	…	…	…	…	EB
V234*	06 42 30.62	−50 53 34.5	…	…	…	…	EB

Table 2
(Continued)

ID …	α (J2000.0) (hh mm ss)	δ (J2000.0) (dd mm ss)	S86 …	D03 …	VM13 …	Paper VI …	Our …
V235*	06 43 14.32	−51 06 45.0	…	…	…	…	EB
V236*	06 41 03.78	−51 54 52.8	…	…	2 (Mis)	…	EB
V237*	06 41 17.39	−51 05 45.3	…	…	5 (Mis)	…	EB

Notes. Col. 1: Identification star; Col. 2: R.A., (α); Col. 3: Decl., (δ); Col. 4: Type as in S86; Col. 5: Type and identification as in D03; Col. 6: Type and identification as in VM13; Col. 7: Identification and type as in Paper VI; Col. 8: Type as in this study. FV—Field variable. RGB—Variable located along the RGB. SV—Suspected variable.

(This table is available in machine-readable form.)

and two probable LPVs. Moreover, in Paper VI we discovered 14 new variables, but by using the new data set, we confirm that only nine of these are new identifications (see the Appendix for details).

Recently Vivas & Mateo (2013, hereafter VM13) performed a detailed investigation of pulsating stars in Carina. They found 38 RRLs, 10 AC variables and more than 340 new SX Phoenicis (SX Phe). Among them 36 (30 RRLs and 6 ACs) are in common with D03 and 41 (32 RRLs, 7 ACs, 2 EBs) with our new catalog. The nine stars listed by VM13 that do not appear in our catalog are listed in Table 7. These variables were not included in the following analysis of RRLs pulsation properties since they are located beyond the Carina tidal radius (see Section 3.1 for a detailed discussion). Concerning SX Phe stars, we confirm the variability for 324 out of 340 known pulsators in Carina and we identified 101 new variables of this class (see Section 5 for details).

In the first column of Table 2 we find the identification number according to S86 and D03. For the newly detected variables in this paper and in Paper VI (208–237) the D03 running number was continued and these stars were also marked with an asterisk in this same table. Columns (2) and (3) list α and δ (J2000.0) coordinates in units of (hh:mm:ss) and (dd:mm:ss), respectively,[12] while the last five columns give S86, D03, VM13, Paper VI and current individual notes. Candidate variable stars for which we could not confirm the variability are given in Table 3.

The current data set included the *BV* images adopted by D03 in their investigation of Carina's variable stars. We confirm their variability analysis and their variable star classification with only a few exceptions. According to our extended data set the variable V161 does not show clear signs of variability. The variable V17 appears to be an EB variable; while the variables V22 and V176 seem to pulsate in the fundamental (RR_{ab}) instead of in the first overtone (RR_c) mode. The variables V31, V61, V77, V126, V127 and V206 were also classified by D03 as RR_{ab} variables and according to our new data they also show the Blazhko effect. Moreover, the variable V74 was classified by D03 as RR_c variable, but according to our new data it is classified as a double-mode pulsator. A more detailed analysis of individual variables is given in the Appendix.

The individual *UBVI* measurements for all the variables in our sample are listed in Table 4. For every variable in our sample the first three columns of the table contain the Heliocentric Julian Date (HJD), the *U*-band magnitude and the photometric error. Columns (4)–(12) give the same information, but for the *B*-, *V*-, and *I*-band measurements. The total number of phase points in the complete data set depends on the photometric band, and they range from 1 to 23 (*U*), from 22 to 203 (*B*), from 38 to 278 (*V*) and from 3 to 92 (*I*). The coverage of the pulsation cycle is optimal in the *B* and *V* bands, modest in the *I* band and poor in the *U* band. The photometric error of individual measurements depends on the photometric band and on seeing conditions. It is also occasionally affected by crowding conditions, but it is on average of the order of 0.02 mag.

Period searches and the phasing of light curves were performed using the procedure adopted by Stetson et al. (2014a), for the galactic Globular Cluster M4. The large time baseline (∼20 years) covered by our data set allowed us to overcome half- and one-day alias ambiguities that can be quite severe in data sets covering limited time intervals. The large time interval covered by the current data set allowed us to provide more precise periods, epochs of maximum light, and luminosity amplitudes for the entire set of variable stars. In particular, the accuracy of the period estimates is related to the period itself and to the time interval covered by the observations. They range from (1×10^{-8}) to (1×10^{-5}) days.

The mean optical magnitudes and the amplitudes in the bands with good time sampling (*B*, *V*) were estimated from fits with a spline under tension.

We already mentioned that the time sampling of both the *U*- and *I*-band light curves is either modest or poor. This means less accurate mean magnitudes and luminosity amplitudes. To overcome this problem for the *I*-band light curves we adopted the method described by Di Criscienzo et al. (2011) based on using the *V*-band light curve as a template and re-scaling the same measurements in amplitude to fit the *I*-band light curves. To accomplish this goal we adopted a visual-to-*I*-band amplitude ratio of 1.58 ± 0.03, obtained by Di Criscienzo et al. (2011) using the literature *V* and *I* light curves of 130 RRLs with good light curve parameters selected from different Galactic globular clusters.

The *U*-band light curves for several variables are poorly sampled, and often there is no coverage across minimum and/or maximum light. In those cases, we adopted as a mean magnitude the median of measurements and we do not provide luminosity amplitudes.

Table 5 lists, from left to right, for every variable in the current data set, the identification, the classification, the epoch of maximum light, the period (days), the intensity-averaged [$\langle U\rangle, \langle B\rangle, \langle V\rangle, \langle I\rangle$] mean magnitudes and the $A(U)$, $A(B)$, $A(V)$, $A(I)$ luminosity amplitudes. For some variables the light curves are poorly sampled, and as explained above for the *U* band, we

[12] The astrometry is on the system of the USNO-A2.0 catalog.

Table 3
Catalog of Candidate Variable Stars that According to the Current Investigation are Not Variable

ID	α (J2000.0)	δ (J2000.0)	S86	D03	This Work
…	(hh mm ss)	(dd mm ss)	…	…	…
V1	06 42 21.90	−50 51 35.0	ab	…	NV
V2	06 42 19.60	−50 45 12.0	SV	…	NV
V5	06 43 19.04	−50 53 29.3	SV	NV	NV
V6	06 43 18.01	−50 46 43.7	SV	NV	NV
V8	06 42 56.44	−50 41 45.6	δScu	NV	NV
V9	06 43 16.00	−51 02 43.6	WUma	NV	NV[a]
V12	06 43 06.20	−50 59 04.6	δScu	NV	NV[b]
V13	06 43 05.02	−50 49 33.0	SV	NV	NV[b]
V15	06 43 00.82	−50 50 28.2	SV	NV	NV
V16	06 42 56.33	−50 54 47.4	SV	NV	NV[b]
V17	06 42 56.39	−51 08 38.0	SV	NV	EB
V18	06 37 30.80	−51 17 31.4	SV	NV[c]	NV
V19	06 42 54.24	−50 44 44.8	SV	NV	NV
V20	06 42 50.97	−50 56 06.7	SV	NV	NV
V21	06 42 46.66	−51 08 50.6	SV	NV	NV
V23	06 42 37.03	−51 03 28.6	ab	…	NV
V28	06 42 26.26	−50 59 44.2	SV	NV[c]	NV[a]
V35	06 42 19.37	−50 48 44.0	SV	NV	NV
V36	06 42 18.15	−51 08 07.6	SV	NV	NV
V37	06 41 52.94	−50 44 11.4	SV	NV	NV[d]
V38	06 42 17.30	−51 07 16.0	SV	NV	NV[b]
V39	06 42 17.21	−51 01 58.0	SV	NV[c]	NV
V42	06 42 14.75	−50 55 36.0	SV	NV	NV[b]
V45	06 42 10.98	−51 12 56.5	SV	NV	NV
V46	06 42 08.71	−50 46 57.3	SV	NV	NV[b]
V48	06 42 08.98	−51 02 40.4	SV	NV	NV
V50	06 42 08.50	−51 02 52.1	SV	NV	NV
V51	06 42 08.32	−51 02 26.7	SV	NV	NV
V52	06 42 07.52	−50 43 08.4	SV	NV	NV
V53	06 42 07.46	−50 51 25.3	SV	NV	NV
V54	06 42 07.54	−51 01 17.0	SV	NV	NV
V55	06 42 31.74	−50 51 56.7	SV	NV	NV[e]
V56	06 42 04.38	−50 49 15.1	SV	NV	NV
V59	06 41 59.71	−50 50 37.3	SV	NV	NV
V62	06 41 57.81	−50 59 53.3	SV	NV	NV[b]
V63	06 41 57.40	−51 03 23.0	SV	NV	NV
V64	06 41 57.17	−50 53 30.0	SV	NV	NV[b]
V66	06 41 53.04	−51 12 38.3	SV	NV	NV
V69	06 41 48.94	−51 02 32.5	c	NV	NV[a]
V70	06 41 48.23	−50 55 01.8	SV	NV	NV
V71	06 41 47.90	−51 03 12.6	SV	NV	NV
V72	06 41 46.89	−51 05 25.3	SV	NV	NV
V76	06 41 39.68	−50 48 56.1	SV	NV	NV[e]
V78	06 40 26.70	−51 08 23.0	SV	…	NV
V79	06 41 38.26	−50 49 03.5	SV	NV	NV
V80	06 41 38.36	−51 04 37.5	SV	NV	NV[b]
V81	06 41 37.70	−51 02 37.2	SV	NV	NV
V82	06 41 37.52	−50 57 41.5	SV	NV	NV[c]
V83	06 41 37.46	−51 01 37.1	SV	NV	NV[c]
V86	06 41 33.86	−50 43 49.3	SV	NV	NV
V88	06 41 31.18	−50 57 56.1	SV	NV	NV
V93	06 40 16.20	−51 10 20.0	SV	…	NV
V94	06 40 14.60	−50 57 20.0	SV	…	NV
V95	06 41 26.76	−50 52 15.0	SV	NV	NV[b]
V96	06 41 24.98	−50 44 11.9	SV	NV	NV
V97	06 40 09.40	−50 54 31.0	SV	…	NV
V98	06 40 08.50	−50 57 17.0	SV	…	NV
V99	06 41 18.87	−50 58 24.8	SV	NV	NV
V100	06 40 05.6	−50 43 48.0	c	…	NV
V101	06 41 18.13	−51 01 28.0	SV	NV	NV
V102	06 41 18.12	−51 10 57.1	SV	NV	NV
V103	06 41 17.40	−50 55 15.3	SV	NV	NV
V104	06 41 16.45	−51 01 08.8	SV	NV	NV[b]
V106	06 41 15.10	−51 08 40.7	SV	NV	NV[b]
V107	06 41 11.36	−51 11 14.8	SV	NV	NV
V108	06 41 10.55	−51 08 19.5	SV	NV	NV
V109	06 41 09.53	−50 59 43.8	SV	NV[a]	NV[a]
V110	06 41 09.18	−51 00 33.7	SV	NV	NV[b]
V111	06 39 56.10	−50 54 36.0	SV	…	NV
V112	06 41 08.80	−51 04 39.3	SV	NV	NV
V113	06 41 08.56	−50 48 21.1	SV	NV	NV
V114	06 41 08.26	−50 54 41.1	SV	NV	NV[b]
V117	06 39 52.60	−51 00 07	SV	…	NV
V118	06 41 01.82	−50 47 22.4	SV	NV	NV[e]
V119	06 41 01.44	−50 52 30.7	SV	NV	NV
V120	06 40 58.83	−50 45 24.4	SV	NV	NV
V121	06 40 57.49	−51 00 41.2	SV	NV	NV
V128	06 40 49.17	−51 00 33.4	SV	…	NV[b]
V130	06 39 35.90	−50 43 13.0	SV	…	NV
V131	06 39 36.50	−51 01 43.0	SV	…	NV
V132	06 39 35.90	−50 54 38.0	SV	…	NV
V134	06 39 35.80	−51 06 54.0	SV	…	NV
V137	06 40 43.01	−50 55 54.3	SV	NV	NV
V139	06 40 39.86	−50 53 22.9	SV	NV	NV
V140	06 40 39.47	−51 07 02.2	SV	NV	NV
V145	06 40 36.06	−50 58 31.1	SV	NV	NV
V146	06 40 34.79	−51 01 51.7	SV	NV	NV
V147	06 40 34.08	−51 11 29.9	SV	NV	NV[b]
V150	06 40 30.73	−50 45 27.9	SV	NV	NV
V152	06 40 29.32	−50 42 14.5	SV	NV[c]	NV[b]
V154	06 40 13.95	−50 42 55.1	SV	NV	NV
V155	06 40 19.68	−50 45 45.4	SV	NV	NV
V156	06 40 17.98	−51 06 02.0	SV	NV	NV
V157	06 40 17.60	−50 58 41.4	SV	NV	NV
V160	06 40 01.42	−51 02 50.3	SV	NV	NV
V161	06 40 00.98	−51 04 06.6	SV	SV	NV[a]
V162	06 40 00.14	−50 44 14.5	SV	NV	NV
V163	06 39 57.08	−50 51 10.6	SV	NV	NV
V166	06 38 29.90	−50 52 41.0	SV	…	NV
V167	06 38 30.30	−50 54 36.0	SV	…	NV
V168	06 38 29.90	−50 54 27.0	SV	…	NV
V169	06 38 29.2	−50 45 05.0	SV	…	NV
V172	06 41 08.38	−50 47 06.8	SV	NV	NV

Notes. Col. 1: Identification star; Col. 2: R.A., (α); Col. 3: Decl., (δ); Col. 4: Type as in S86; Col. 5: Type as in D03; Col. 6: Type as in this study. NV—No variability detected. SV—Suspected variable.
[a] Possible blend.
[b] Located close to a bright or faint star.
[c] Possible field galaxy.
[d] Saturated star.
[e] Faint star.

(This table is available in machine-readable form.)

adopted as a mean magnitude the median of measurements and do not provide luminosity amplitudes. Note that for RR_d variables the same observables and the period ratios, P_0/P_1, are listed in Table 6. For these stars we did not perform the analysis of pulsational parameters in the *U*-band, because the *U*-band light curves are not well sampled.

Figures 1 and 2 show the IS and a zoom of the position of RRLs in the *V*, $(B-V)$ CMD, respectively. Red and green circles display fundamental and first-overtone RRLs. Orange triangles and gray circles mark double-mode pulsators and

Table 4
Photometry of the Carina Variable Stars

HJD	U	σ_U	HJD	B	σ_B	HJD	V	σ_V	HJD	I	σ_I
V7											
53351.7001	21.50	0.03	51552.5736	21.33	0.02	51552.5669	20.90	0.02	53351.7698	20.38	0.02
53351.7129	21.64	0.03	51552.5854	21.40	0.02	51552.5786	20.90	0.01	53351.7745	20.40	0.02
53351.7256	21.59	0.03	51552.5971	21.43	0.02	51552.5904	20.94	0.02	53351.7791	20.38	0.02
53351.7387	21.59	0.04	51552.6089	21.43	0.02	51552.6021	20.92	0.01	53351.7838	20.37	0.02
53351.7515	21.62	0.04	51552.6209	21.47	0.01	51552.6141	21.03	0.01	53351.7885	20.43	0.02
53351.7642	21.68	0.03	51552.6327	21.49	0.02	51552.6259	20.99	0.02	53351.7931	20.35	0.02
53359.7729	21.39	0.03	51552.6445	21.53	0.02	51552.6378	21.04	0.01	53351.7978	20.43	0.02
53359.7858	21.14	0.02	51552.6562	21.53	0.02	51552.6495	21.04	0.02	53359.6762	20.39	0.01
53359.7992	20.75	0.02	51552.6681	21.56	0.02	51552.6613	21.08	0.01	53359.6808	20.39	0.02
53359.8121	20.45	0.02	51552.6798	21.54	0.02	51552.6731	21.04	0.02	53359.6855	20.34	0.02
			51552.6916	21.58	0.02	51552.6849	21.10	0.02	53359.6901	20.36	0.01

(This table is available in its entirety in machine-readable form.)

candidate Blazhko RRLs, while cyan symbols show the location of AC variable stars. Yellow and blue squares represent RGB and LPV variables, while black stars display the locations of the EBs (see Table 2). Finally, magenta and black pentagons show the RRLs and ACs in the catalog of VMC13 and not in common with our catalog. Blue and red lines display the theoretical IS boundaries predicted by radial nonlinear convective pulsation models for ACs (Fiorentino et al. 2006) and RRLs (Marconi et al. 2015, hereafter M2015). Theoretical predictions were computed assuming a metal abundance of $Z = 0.0001$ (ACs) and of $Z = 0.001$ (RRLs). Theory was transformed into the observational plane using the bolometric corrections and the color–temperature relations provided by Cardelli et al. (1989). We also adopted a true distance modulus of $\mu = (20.09 \pm 0.07)$ mag (Coppola et al. 2013) and a reddening of $E(B - V) = 0.03$ mag (Monelli et al. 2003). The agreement between theory and observations appears, within the errors, quite good both for RRLs and ACs. In the above figures the two bright RR_{ab} stars (V158, V182) were defined as peculiar RRLs in Paper VI. We also note the presence of two RR_{ab} (V170, V227) that appear anomalously blue. These stars have poorly sampled light curves and uncertain pulsational parameters. In particular, the number of measurements we have for the variable V170 is too small to fit the light curve and to estimate the luminosity amplitude (see the Appendix for details). These four stars are labeled and marked in Figure 2 with blue crosses.

Moreover, we identified 101 new SX Phe. Their pulsation properties, their light curves and their position in the V, $(B - V)$ CMD are discussed in Section 5.

3. PULSATION PROPERTIES

Figure 3 shows the *BVI* light curves for fundamental (left) and first overtone (middle) RRLs plus ACs (right). The different data sets were plotted with different colors. The light curves of RR_d variables are plotted in Figure 4. The complete atlas of light curves, including the U-band data, is available in the online edition of the paper.

3.1. Bailey Diagram

The left panels of Figure 5 display the Bailey diagram—amplitude versus period—for RRLs. From top to bottom the different panels show amplitudes in the B (top), V (middle) and I (bottom) bands. The Bailey diagram is a very good diagnostic for splitting fundamental and first overtones. The transition period between low-amplitude, short-period RR_c and large-amplitude, long-period RR_{ab} is located around $\log P \sim -0.35/-0.30$ ($P \sim 0.45$–0.5 days). The RR_{ab} display a steady decrease in amplitude when moving toward longer periods. On the other hand, the RR_c show a "bell-shaped" (Bono et al. 1997a) or a "hairpin" (Kunder et al. 2013) distribution. The Bailey diagram is also used to constrain the Oosterhoff class (see, e.g., Bono et al. 1997b) of stellar systems hosting sizable samples of RRLs. The middle panel shows the comparison between RR_{ab} in the V-band with the empirical relations provided by (Clement & Shelton 1999, dashed lines) and by Cacciari et al. (2005, black solid line). The former relations are based on both OoI and OoII GCs, while the latter are only for OoI GCs. The comparison indicates that Carina can be classified either as an OoI or as an Oosterhoff intermediate system, since for periods longer than $\log P > -0.2$ there is a group of RR_{ab} that, at fixed period, attains larger luminosity amplitudes. On the other hand, the amplitudes typical of RR_c variables in OoII GCs (Kunder et al. 2013, blue solid line) agree quite well the current data.

In Paper VI we classified Carina, on the basis of the mean period of fundamentalized RRLs, as an OoII system. Indeed, we found $\langle P_{\rm RR} \rangle = 0.60 \pm 0.01$ days ($\sigma = 0.07$). Including the new discovered RR_{ab} variables we find that the mean period of fundamental RRLs is $\langle P_{\rm RR} \rangle = 0.637 \pm 0.006$ days ($\sigma = 0.05$). This estimate suggests that Carina is closer to an OoII stellar systems, since OoII GCs show mean fundamental periods of $\langle P \rangle \sim 0.65$ days, while the OoI GCs show shorter periods, namely $\langle P \rangle \sim 0.55$ days. We have also computed the ratio between the number of RR_c and the total number of RRLs, and we found $N_c/(N_{ab} + N_c) \sim 0.14$, i.e., a fraction of RR_c variables that is more typical of OoI (~17%) than OoII (~44%) GCs. The above evidence indicates that the Oosterhoff classification of Carina depends on the adopted diagnostic. This means that the Oosterhoff classification should be cautiously treated, since it depends on the adopted diagnostic on the completeness and size of the RRL sample and on the morphology of the HB (Fiorentino et al. 2015a).

The data plotted in Figure 5 also show mixed-mode pulsators, the so-called RR_d variables. These are radial variables oscillating simultaneously in at least two different pulsation modes. The RR_d typically oscillate in the first overtone and in the fundamental mode, and the former mode is usually stronger than the latter (e.g., Smith 2006), but there are

Table 5
Pulsation Properties of Carina Variable Stars

ID	Type	Epoch[a]	Period (day)	⟨*U*⟩[b]	⟨*B*⟩[b]	⟨*V*⟩[b]	⟨*I*⟩[b]	*A*(*U*)	*A*(*B*)	*A*(*V*)	*A*(*I*)
3	ab	52351.2771	0.5786581	21.30[c]	21.127	20.771	20.210	…	1.256	1.012	0.637
4	c	51548.6519	0.3973509	21.243	20.995	20.685	20.234	0.513	0.663	0.565	0.356
7	ab	51548.7025	0.6033121	21.43[c]	21.104	20.729	20.212	…	1.278	1.087	0.685
10	ab	51548.7378	0.5845143	21.158	21.070	20.724	20.203	0.712	1.367	1.095	0.690
14	AC	51548.9240	0.4766975	20.510	20.265	19.994	19.507	0.838	0.886	0.745	0.469
17	EB	51548.5693	0.3933393	22.03[c]	20.968	19.606	17.705	…	0.092	0.086	0.059
22	ab	51549.0012	0.6380630	21.209	21.155	20.746	20.133	0.757	0.709	0.518	0.326
24	ab	51548.5844	0.6181987	21.48[c]	21.088	20.730	20.126	…	0.909	0.723	0.456
25	Bl	52351.7201	0.5956510	21.20[c]	21.077	20.718	20.128	…	0.993	0.856	0.539
27	AC	51549.1519	1.0203875	20.23[c]	19.817	19.376	18.820	…	1.118	0.971	0.612
29	AC	51549.2591	0.7178952	19.297	19.283	19.013	18.608	1.152	1.015	0.811	0.511
30	ab	51548.7682	0.6188105	21.57[c]	21.179	20.774	20.136	…	0.893	0.699	0.441
31	Bl	51548.7359	0.6457949	21.39[c]	21.154	20.750	20.093	…	0.598	0.468	0.295
32	ab	51548.6507	0.6150517	21.44[c]	21.108	20.723	20.096	…	0.875	0.743	0.468
33	AC	51549.1187	0.5836254	20.47[c]	20.055	19.735	19.155	…	0.779	0.645	0.406
34	ab	51548.8657	0.5869516	21.44[c]	21.108	20.767	20.281	…	1.281	0.993	0.625
40	c	51548.6092	0.3926228	21.183	21.125	20.781	20.223	0.429	0.525	0.441	0.278
41	AC	51548.5461	1.0381530	19.77[c]	19.393	19.091	18.577	…	1.552	1.215	0.765
43	c	51548.9153	0.2992499	21.31[c]	20.945	20.741	20.353	…	0.567	0.477	0.300
44	ab	52351.3257	0.6264277	20.89[c]	21.109	20.740	20.160	…	1.181	0.963	0.607
47	c	51548.7090	0.3237674	21.26[c]	20.996	20.762	20.355	…	0.760	0.619	0.390
49	ab	51548.8332	0.6815073	21.30[c]	21.106	20.690	20.052	…	0.537	0.419	0.264
57	ab	51548.5449	0.6129016	21.294	21.195	20.783	20.185	0.854	0.854	0.671	0.423
58	ab	52351.7078	0.6194599	21.119	21.079	20.690	20.075	0.688	0.839	0.644	0.406
60	ab	51549.4418	0.6094132	21.341	21.148	20.746	20.157	0.539	1.016	0.808	0.509
61	Bl	51548.8037	0.6213493	21.28[c]	21.070	20.674	20.088	…	0.936	0.795	0.501
65	ab	51548.6491	0.6517109	21.171	21.079	20.707	20.109	1.242	1.069	0.922	0.581
67	ab	51548.9560	0.60372385	21.064	21.100	20.726	20.136	0.763	0.856	0.716	0.451
68	ab	51548.5512	0.6787359	21.43[c]	21.158	20.721	20.091	…	0.430	0.352	0.222
73	ab	51548.5572	0.5695182	21.11[c]	21.100	20.756	20.184	…	1.324	1.134	0.715
75	ab	52345.7593	0.5912161	21.209	21.192	20.746	20.164	0.757	0.682	0.538	0.339
77	Bl	51548.6782	0.6043226	21.38[c]	21.101	20.730	20.138	…	1.170	0.837	0.527
84	ab	51548.9285	0.6166815	21.01[c]	21.082	20.722	20.107	…	0.954	0.795	0.501
85	ab	51548.6088	0.6405248	21.078	21.068	20.666	20.065	0.594	0.889	0.654	0.412
87	AC	51548.9360	0.8556130	19.144	18.975	18.732	18.353	0.526	0.644	0.478	0.301
90	ab	51548.6598	0.6313625	21.46[c]	21.135	20.724	20.145	…	0.807	0.636	0.401
91	ab	51548.7635	0.7180705	21.164	21.105	20.684	20.023	0.600	0.751	0.579	0.365
92	ab	51548.7778	0.6301283	21.112	21.157	20.737	20.124	0.677	0.760	0.619	0.390
105	ab	51548.4033	0.6323014	20.99[c]	21.108	20.699	20.085	…	0.834	0.680	0.428
115	AC	51549.4635	1.0109789	19.284	19.016	18.703	18.196	0.547	0.841	0.691	0.435
116	ab	51548.2506	0.6833133	21.15[c]	21.157	20.758	20.194	…	0.938	0.727	0.458
122	ab	51548.8260	0.6314692	21.096	21.066	20.673	20.065	0.905	0.865	0.734	0.462
123	ab	51548.5547	0.6749693	21.35[c]	21.079	20.674	20.065	…	0.829	0.689	0.434
124	ab	51548.9470	0.5917211	21.34[c]	21.043	20.672	20.139	…	1.117	0.899	0.566
125	ab	51548.4329	0.5940963	20.94[c]	20.964	20.641	20.073	…	1.332	1.091	0.688
126	Bl	51548.5952	0.5570972	21.23[c]	21.072	20.741	20.160	…	1.070	0.917	0.578
127	Bl	51548.3900	0.6262952	21.22[c]	21.140	20.744	20.163	…	0.694	0.506	0.319
129	AC	51549.2201	0.6301768	19.477	19.368	19.107	18.698	0.788	1.006	0.802	0.505
133	ab	52351.8941	0.6123127	21.398	21.160	20.776	20.237	1.463	1.011	0.813	0.512
135	ab	51548.9530	0.5909193	21.30[c]	20.982	20.624	20.091	…	1.213	0.945	0.596
136	ab	51548.1625	0.631613	21.24[c]	21.099	20.691	20.064	…	0.731	0.575	0.362
138	ab	51548.3027	0.6392611	21.12[c]	21.110	20.704	20.094	…	0.691	0.549	0.346
141	ab	51548.3418	0.6353340	21.20[c]	21.143	20.737	20.144	…	0.688	0.532	0.335
142	c	51548.4286	0.3635433	21.05[c]	21.004	20.734	20.254	…	0.677	0.548	0.345
143	ab	51548.6506	0.6095789	21.297	21.063	20.674	20.116	1.336	0.934	0.763	0.481
144	c	51548.9292	0.3933566	21.086	20.969	20.661	20.153	0.414	0.545	0.427	0.269
148	c	51548.7335	0.3266545	21.01[c]	20.656	20.444	20.084	…	0.701	0.592	0.373
149	AC	51548.5879	0.9177072	20.96[c]	20.444	20.077	19.488	…	1.074	0.888	0.560
151	c	51548.8155	0.3418011	21.35[c]	21.125	20.842	20.374	…	0.584	0.465	0.293
153	ab	51548.4220	0.6603692	21.076	21.072	20.674	20.083	0.717	0.670	0.539	0.339
158	ab	51548.5230	0.6324566	20.902	20.785	20.330	19.642	0.715	0.625	0.458	0.288
159	ab	51548.5223	0.5751520	20.94[c]	21.033	20.702	20.171	…	1.164	0.976	0.615
164	ab	51548.3880	0.6339196	21.38[c]	21.095	20.718	20.104	…	0.709	0.569	0.359
165	ab	51548.6742	0.5790136	20.57[c]	21.057	20.751	20.223	…	1.315	1.081	0.681

Table 5
(Continued)

ID	Type	Epoch[a]	Period (day)	⟨U⟩[b]	⟨B⟩[b]	⟨V⟩[b]	⟨I⟩[b]	A(U)	A(B)	A(V)	A(I)
170	ab	51543.0033	0.59[d]	21.06[c]	21.04[c]	20.79[c]	20.26[c]	…	…	…	…
171	ab	51542.6010	0.66[d]	21.48[c]	21.14[c]	20.76[c]	20.11[c]	…	…	…	…
173	RGB	51549.1135	0.657779	20.79[c]	19.573	18.542	17.25[c]	…	0.095	0.094	…
174	ab	51548.5789	0.6531203	21.22[c]	21.175	20.756	20.152	…	0.507	0.417	0.263
175	c	51548.8389	0.3923778	21.23[c]	21.068	20.739	20.263	…	0.532	0.454	0.286
176	ab	51549.4881	0.764565	21.33[c]	21.160	20.715	20.061	…	0.264	0.212	0.133
178	AC	51549.0958	1.0155700	19.25[c]	19.535	19.207	18.768	…	1.512	1.244	0.784
179	ab	51548.7597	0.6637945	21.26[c]	21.155	20.719	20.081	…	0.247	0.196	0.124
181	c	51549.0010	0.2794913	21.16[c]	20.996	20.781	20.350	…	0.095	0.076	0.048
182	ab	51548.1454	0.7889722	20.48[c]	20.588	20.178	19.571	…	0.380	0.323	0.204
183	ab	51548.7509	0.612302	21.21[c]	20.963	20.596	20.013	…	0.615	0.508	0.320
184	c	51548.4830	0.3951290	21.165	21.011	20.714	20.213	0.499	0.539	0.422	0.266
185	ab	51548.5511	0.6209146	21.31[c]	21.097	20.731	20.155	…	0.871	0.678	0.427
187	AC	51549.0083	0.9502923	19.42[c]	19.440	19.166	18.674	…	1.389	1.154	0.727
188	ab	51548.6637	0.5973773	21.19[c]	21.019	20.665	20.143	…	1.290	1.127	0.710
189	ab	51548.8546	0.7023692	21.22[c]	21.028	20.639	20.044	…	0.771	0.647	0.407
190	AC	51549.2923	1.1647103	19.622	19.478	19.137	18.547	0.848	1.546	1.294	0.815
191	ab	51548.7011	0.6502894	21.066	21.091	20.686	20.114	0.633	0.711	0.561	0.354
193	AC	51549.1506	0.4263580	19.68[c]	19.530	19.284	18.900	…	0.172	0.131	0.082
194	FV	51549.2016	0.2645828	16.32[c]	16.076	15.879	15.525	…	0.133	0.123	0.072
195	ab	51548.5576	0.6189680	21.18[c]	21.140	20.769	20.143	…	0.646	0.483	0.304
196	ab	51548.2819	0.665989	21.213	21.081	20.676	20.132	0.740	0.500	0.410	0.258
197	c	51548.7640	0.2961717	21.24[c]	20.959	20.739	20.331	…	0.390	0.312	0.197
199	ab	51548.1840	0.769925	20.976	20.999	20.574	19.942	0.322	0.485	0.406	0.256
200	ab	51548.5254	0.6373468	21.24[c]	21.156	20.738	20.101	…	0.359	0.289	0.182
201	ab	51548.5885	0.7222435	21.32[c]	21.133	20.730	20.084	…	0.762	0.632	0.398
203	AC	51549.2587	0.9398875	19.924	19.820	19.427	18.838	0.736	1.052	0.812	0.511
204	ab	51548.8631	0.6332687	21.40[c]	21.121	20.725	20.094	…	0.654	0.545	0.344
205	AC	51549.1382	0.3833676	20.189	19.891	19.668	19.281	0.399	0.156	0.145	0.091
206	Bl	51548.5382	0.587812	21.48[c]	21.069	20.700	20.113	…	1.192	1.053	0.664
208	ab	52352.0043	0.656594	21.39[c]	21.125	20.721	20.073	…	0.619	0.484	0.305
214	Bl	52352.3784	0.6391863	21.17[c]	21.031	20.674	20.077	…	1.041	0.753	0.475
216	AC	51549.6831	1.079230	19.32[c]	19.258	18.853	18.201	…	0.427	0.303	0.191
217	AC	51549.7742	0.9109459	18.71[c]	18.864	18.600	18.156	…	0.839	0.676	0.425
218	AC	52351.7154	1.0086934	20.44[c]	20.141	19.742	19.224	…	0.571	0.485	0.305
219	AC	52352.9984	1.365517	19.58[c]	19.277	18.879	18.252	…	0.476	0.387	0.244
220	EB	51548.7085	0.37264174	15.59[c]	15.364	14.681	13.872	…	0.733	0.750	0.663
221	WUma	51549.0298	1.783454	22.01[c]	20.551	19.228	17.43[c]	…	0.165	0.150	…
222	LP	51519.2828	329	21.70[c]	19.35[c]	17.42[c]	15.66[c]	…	…	…	…
223	ab	52352.8734	0.660937	21.24[c]	21.105	20.715	20.061	…	0.309	0.257	0.162
224	LP	52401.0706	685	20.10[c]	21.05[c]	20.47[c]	19.83[c]	…	…	…	…
226	ab	51549.3101	0.669846	21.12[c]	21.086	20.698	20.082	…	0.432	0.322	0.203
227	ab	51550.7387	0.5594254	…	21.265	20.940	20.274	…	0.876	0.607	0.382
228	ab	51548.2822	0.6290089	20.86[c]	21.082	20.713	20.083	…	0.600	0.500	0.315
229	ab	51548.3681	0.6626030	21.02[c]	21.085	20.681	20.072	…	0.449	0.342	0.235
230	AC	52351.3174	1.0025734	19.73[c]	19.580	19.2546	18.663	…	1.353	1.074	0.677
231	EB	51549.5699	2.3831781	21.19[c]	21.36[c]	21.23[c]	20.97[c]	…	…	…	…
232	EB	51548.7853	0.4142902	17.28[c]	16.44[c]	15.44[c]	14.14[c]	…	…	…	…
233	EB	51548.8868	0.6378688	22.48[c]	22.37[c]	22.26[c]	22.14[c]	…	…	…	…
234	EB	51548.4601	0.5274709	24.44[c]	22.59[c]	21.14[c]	18.99[c]	…	…	…	…
235	EB	51548.6759	0.6539230	18.54[c]	18.43[c]	17.74[c]	16.89[c]	…	…	…	…
236	EB	51548.7125	0.3747540	22.35[c]	22.41[c]	22.35[c]	22.32	…	…	…	…
237	EB	51548.7915	0.4083364	22.03[c]	22.003	21.761	21.49[c]	…	0.323	0.314	…

Notes.
[a] Epoch of maximum light.
[b] Intensity-averaged magnitudes.
[c] Median of individual magnitude measurements.
[d] Not enough data to fit a light curve, uncertain parameters.

exceptions (Clementini et al. 2004). On the other hand, Classical Cepheids display a wide range of mixed-mode pulsators among the overtones and fundamental mode (Soszynski et al. 2008; Soszyñski et al. 2010), suggesting that surface gravity and effective temperature might play fundamental roles in driving the occurrence of such a phenomenon. Figure 6 shows the comparison in the Bailey diagram between the current observations and predicted amplitudes. Pulsation

Table 6
Pulsation Properties of Carina RR_d Variable Stars

ID	Epoch	P_0 (days)	P_1/P_0 (days)	$\langle B \rangle$ (mag)	$\langle V \rangle$ (mag)	$\langle I \rangle$ (mag)	$A(B_0)$ (mag)	$A(B_1)$ (mag)	$A(V_0)$ (mag)	$A(V_1)$ (mag)	$A(I_0)$ (mag)	$A(I_1)$ (mag)
V11	51548.9191	0.543689	0.745854	21.080	20.766	20.247	0.548	0.341	0.451	0.339	0.28	0.21
V26	51548.9291	0.562177	0.745703	20.990	20.670	20.162	0.604	0.488	0.610	0.395	0.39	0.25
V74	51548.7140	0.533702	0.747205	21.059	20.712	20.246	0.607	0.222	0.567	0.263	0.36	0.17
V89	51548.6377	0.519403	0.746522	21.102	20.770	20.222	0.408	0.384	0.524	0.278	0.33	0.17
V192	51549.0958	0.541694	0.748661	21.030	20.720	20.252	0.753	0.525	0.600	0.345	0.38	0.22
V198	51548.6238	0.530551	0.745534	21.058	20.710	20.192	0.664	0.323	0.506	0.334	0.32	0.21
V207	51549.1028	0.541156	0.746387	21.122	20.782	20.215	0.621	0.548	0.637	0.349	0.40	0.22
V210	52351.5738	0.57324	0.75286	21.010	20.639	20.048	0.474	0.275	0.418	0.218	0.26	0.14
V225	52351.8655	0.57688	0.74610	20.960	20.641	20.147	0.776	0.363	0.575	0.324	0.36	0.20

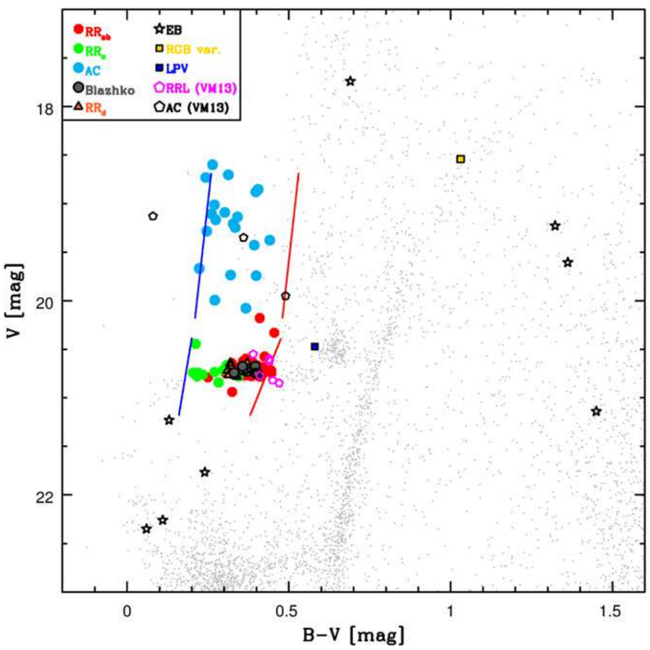

Figure 1. Position of variable stars in V, $(B - V)$ CMD. Red and green circles display fundamental and first-overtone RRLs. Orange triangles and gray circles mark double-mode pulsators and candidate Blazhko RRLs. Cyan symbols show ACs. Yellow and blue squares display candidate RGB and LPV variables, while black stars show the EB variables. Two EBs, not members of Carina, fall outside the plot limits; their colors and magnitudes are given in Table 5.

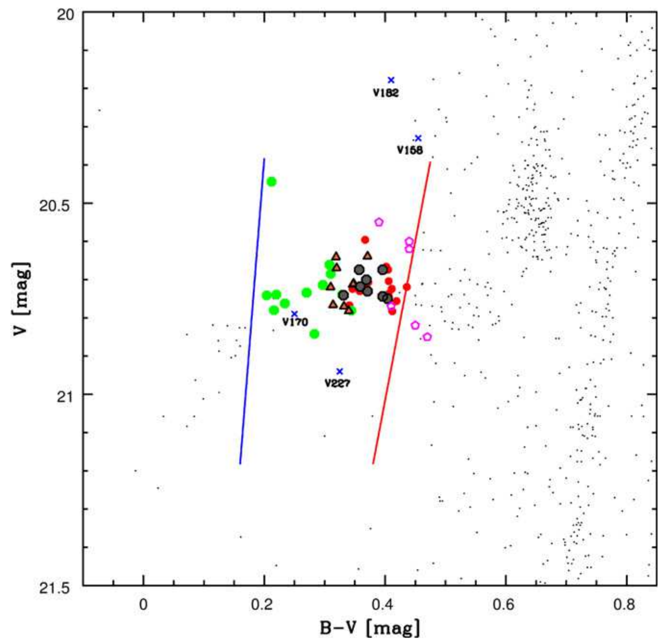

Figure 2. Same as Figure 1, but zoomed on the CMD region located around the RR Lyrae instability strip.

prescriptions rely on a large set of RRL models recently provided by M2015. The black solid and dotted lines display predicted amplitudes for the sequence of metal-poor ($Z = 0.0001$, $Y = 0.245$) models constructed by assuming a stellar mass of 0.80 $M_\odot$ and two different luminosity levels. The black solid line shows predictions for the Zero-Age-Horizontal-Branch (ZAHB) luminosity level ($\log(L/L_\odot) = 1.76$), while the dotted line for a brighter luminosity level ($\log(L/L_\odot) = 1.86$). The purple lines display the same predictions, but for a slightly more metal-rich chemical composition ($Z = 0.0003$, $Y = 0.245$; $M = 0.716$ $M_\odot$, $\log(L/L_\odot) = 1.72$ and 1.82).

The predicted amplitudes appear to be slightly larger, at fixed pulsation period, when compared with observations. This is a limit in the current theoretical framework, since the amplitudes are tightly correlated with the efficiency of convective transport. In passing we note that the comparison between predicted and observed luminosity amplitudes is hampered by the current theoretical uncertainties in the treatment of the time dependent convective transport. We current adopt a mixing length parameter of $\alpha = 1.5$ (see Marconi et al. 2011). Larger values cause a steady decrease in the luminosity amplitude (see Di Criscienzo et al. 2004). Indeed, observed amplitudes attain, at fixed period smaller amplitudes. This applies to both fundamental and first overtone variables. Moreover, we are assuming that observed light curves have a good sampling around the phases of minimum and maximum light. However, the comparison shows two interesting features. (i) The predicted amplitudes for FO pulsators show a larger dependence on metal content than fundamental pulsators. (ii) The regular pulsators display, at fixed pulsation period, a small spread in amplitudes. The current predictions suggest that their evolutionary status is quite homogenous, since they appear to be located to the ZAHB luminosity level.

Carina was previously known to host six RR_d variables: V11, V26, V89, V192, V198, V207 (D03); in the current analysis we discovered other three double-mode pulsators: V74, V210, and V225. To further understand their nature, and in particular to properly define the location of RR_d pulsators in the Bailey diagram, we estimated both primary (first overtone)

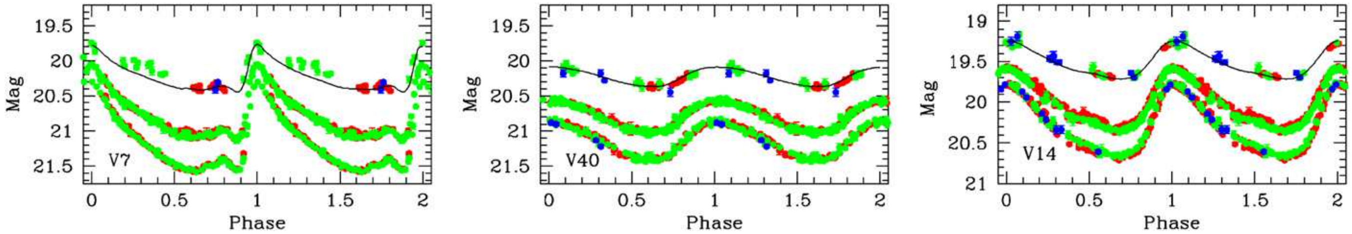

Figure 3. *BVI* light curves for selected Carina variables. We selected one RR_{ab} (V7, left panel), one RR_c (V40, middle panel), and one AC (V14, right panel). Red, green, blue, and yellow filled circles display different data sets: MOSAIC2@CTIO, WFI@MPI/ESO, Tek2K-I@CTIO, and FORS1@ESO/VLT. Black lines are the fits of the light curves. For the *I* band they are the template light curves obtained by properly scaling the *V*-band light curve according to the procedure described in Section 2. The *BVI* plus the *U*-band light curves for the the entire sample of variables are given in the electronic edition of the journal.

(The complete figure set (15 images) is available.)

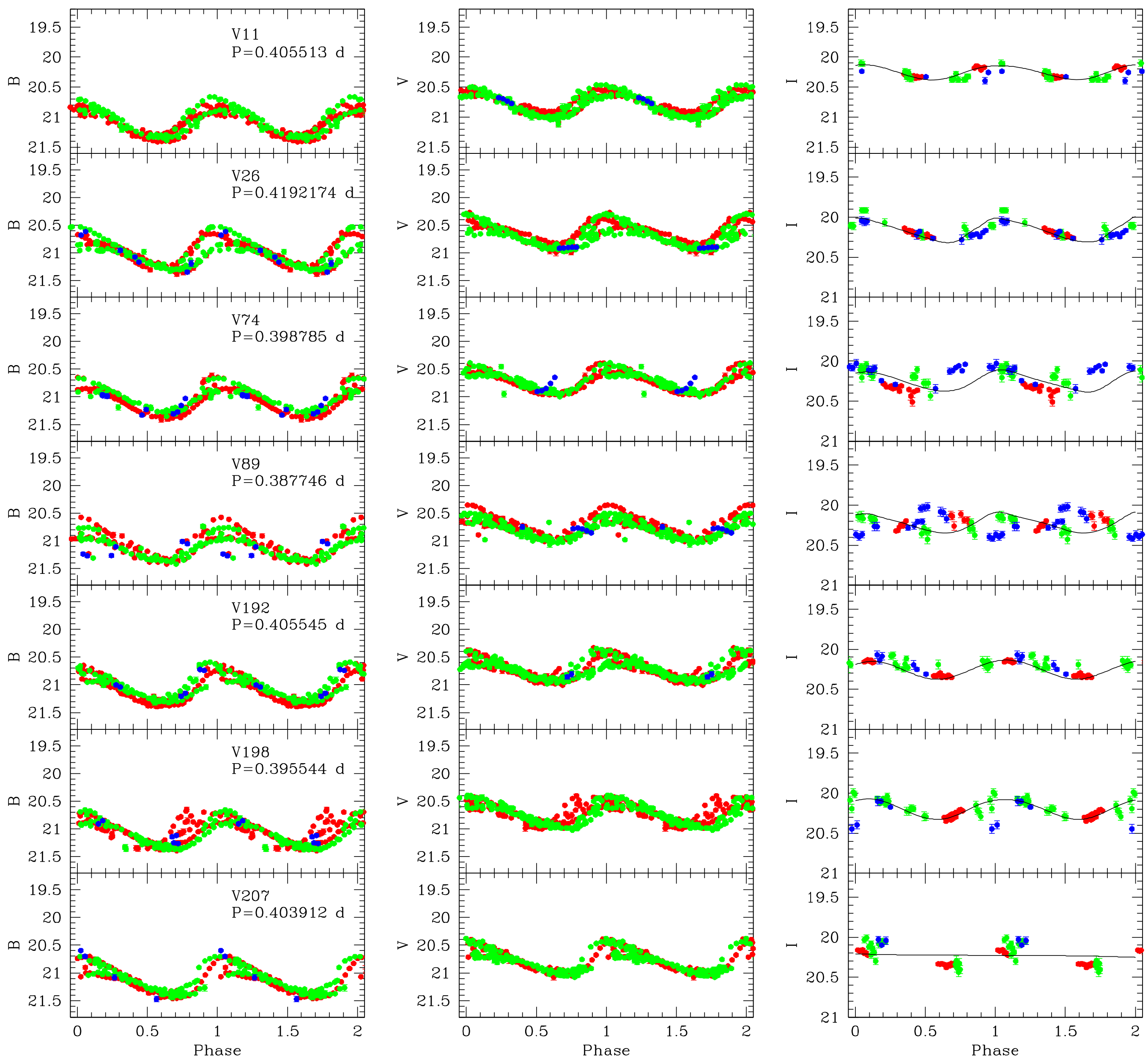

Figure 4. Same as Figure 3, but for the *BVI* light curves of the nine RR_d stars in our sample.

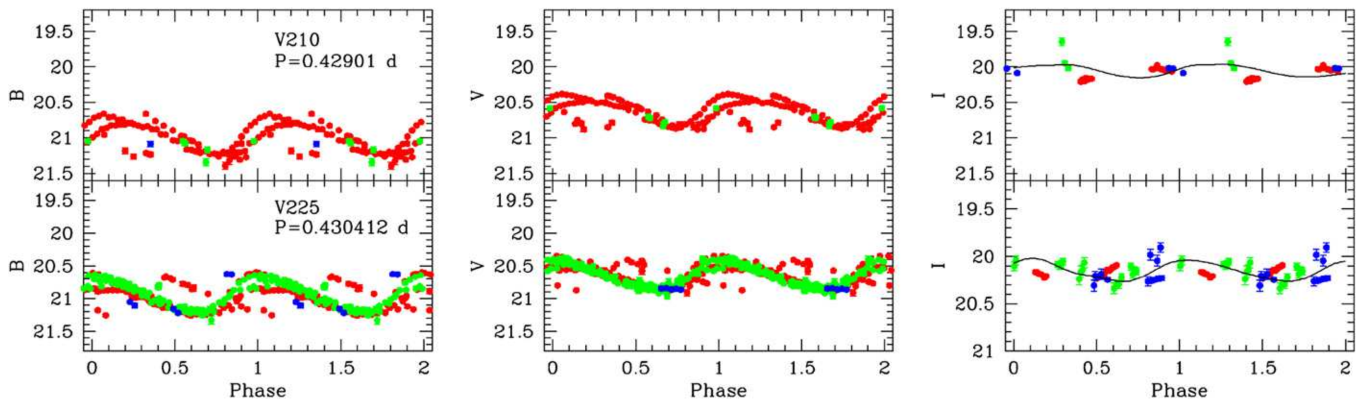

Figure 4. (Continued.)

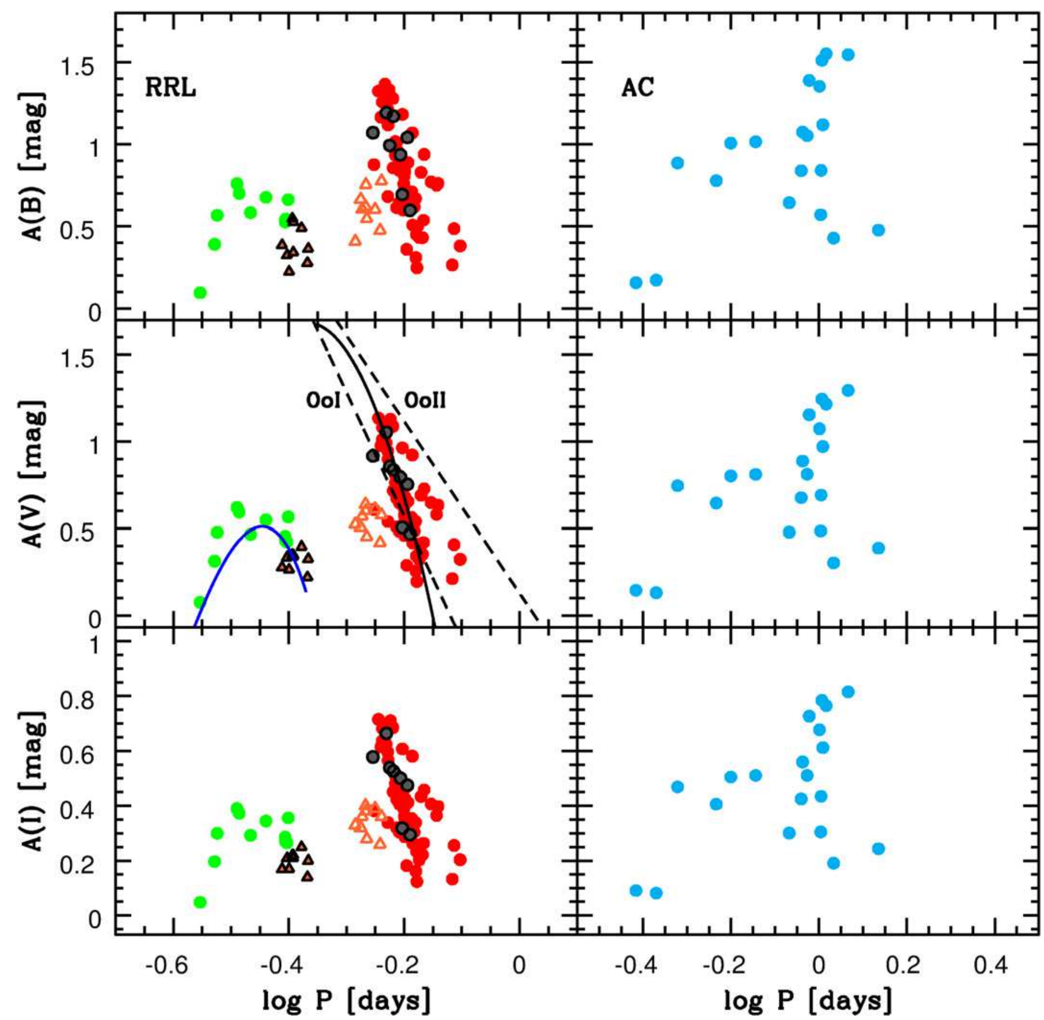

Figure 5. From top to bottom Bailey diagram in *B* (top), *V* (middle), and *I* band (bottom) for Carina RRLs (left) and ACs (right). The dashed lines plotted in the middle left panel display OoI and OoII relations for fundamental pulsators in Galactic globular clusters according to Clement & Shelton (1999), while the black solid line shows the relation for OoI cluster according to Cacciari et al. (2005). The blue solid line shows the relation for OoII first overtone cluster variables provided by Kunder et al. (2013). Symbols are the same as in Figure 1. Note that double-mode variables have been plotted using periods and amplitudes of both primary (first overtone, filled orange triangles) and secondary (fundamental, empty orange triangles) components.

and secondary (fundamental) periods and decomposed their light curves. Indeed, the quality of the photometry allowed us to estimate not only the "global luminosity amplitude," but also the amplitude of both fundamental (open orange triangles) and first overtone mode (filled orange triangles). Table 6 gives from left to right their periods, mean magnitudes and amplitudes in the *BVI* bands. To our knowledge this is the first time in which we can associate to the two modes of double-mode variables their individual luminosity amplitudes. The data plotted in the left panels of Figure 5 indicate that the primary components

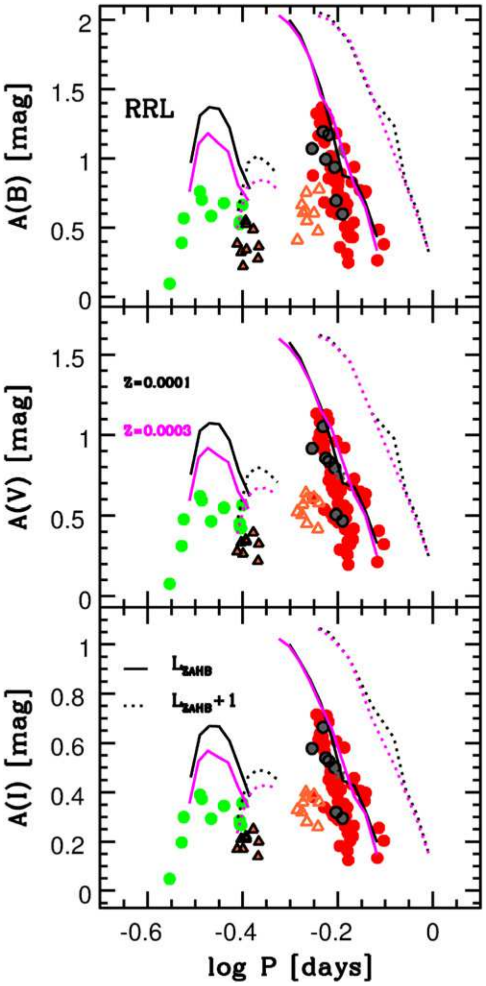

Figure 6. Same as left panels of Figure 5, but the comparison is between observations and predicted luminosity amplitude provided by M2015. The solid lines display predicted amplitude for F and FO models constructed by assuming a stellar mass of $M = 0.80\ M_{\odot}$ a metal-poor chemical composition ($Z = 0.0001$, $Y = 0.245$) and Zero-Age-Horizontal-Branch luminosity level ($\log(L Ł_{\odot}) = 1.76$). The black dotted lines display the same predictions, but for models constructed by assuming a brighter luminosity level ($\log(L/L_{\odot}) = 1.86$). The purple lines display the same pulsation predictions, but for pulsation models constructed by assuming a less metal-poor chemical composition ($Z = 0.0003$, $Y = 0.245$).

(first overtone) are located in the long period tale ($\log P \sim -0.4$) of single mode first overtone variables. Moreover, the secondary components (fundamental) are located in the short period tale ($\log P \sim -0.25$) of single mode fundamental variables. This evidence is further supported by their mean colors. The mean color of RR_d is systematically redder ($B - V \sim 0.33$ mag) than the color range covered by RR_c variables ($0.2 \leqslant B - V \leqslant 0.35$ mag) and systematically bluer than the typical color range of RR_{ab} variables ($0.3 \leqslant B - V \leqslant 0.5$ mag).

The pulsation and evolutionary status of the RR_d variables depends on their evolutionary direction and on their position in the so-called OR region (Bono et al. 1997b). In this context it is worth mentioning that RRLs in dwarf spheroidal galaxies appear to lack High Amplitude Short Period (HASP) fundamental variables (Stetson et al. 2014b; Fiorentino et al. 2015a), thus resembling Oosterhoff II globular clusters in the Milky Way (Bono et al. 1997b).

Table 7
Pulsation Properties for the Nine Extra-tidal Variables (Six RRLs, Four ACs) Identified by VM13

ID	Type	P (days)	$\langle B \rangle$ (mag)	$\langle V \rangle$ (mag)	$A(B)$ (mag)	$A(V)$ (mag)
RRL–1	ab	0.629	20.94	20.55	0.55	0.45
RRL–2	ab	0.523	21.04	20.60	0.83	0.65
RRL–3	ab	0.544	21.06	20.62	0.56	0.46
RRL–4	c	0.204	21.32	20.85	0.17	0.24
RRL–5	c	0.107	21.27	20.82	0.14	0.27
RRL–38	c	0.189	21.18	20.77	0.41	0.31
AC–1	…	0.186	20.44	19.95	0.21	0.20
AC–9	…	0.476	19.21	19.13	0.36	0.55
AC–10	…	0.163	19.71	19.35	0.18	0.32

The occurrence of a good sample of RR_d variables in Carina seems to suggest that this region of the Bailey diagram might be populated by mixed-mode variables. Obviously, the occurrence of RR_d variables depends on the topology of the IS, but also on the evolutionary properties (extent in temperature of the so-called blue hook) and, in particular, on the occurrence of the hysteresis mechanism (van Albada & Baker 1971; Bono et al. 1995; Fiorentino et al. 2015a; Marconi et al. 2015) when moving from more metal-poor to more metal-rich stellar structures.

The Blazhko RRLs plotted in Figure 5 also appear to be located in a very narrow period range. No firm conclusion can be reached concerning the distribution in the Bailey diagram of Blazhko RRLs, since the sample size is quite limited and also because the Blazhko cycle is poorly sampled.

The above findings further support the crucial role played by cluster and galactic RRLs to constrain the topology of the IS and to investigate the evolutionary and pulsation status of exotic objects like RR_d and Blazhko RRLs.

The right panels of Figure 5 show the distribution of Carina ACs in the same Bailey diagrams as the RRLs. Their properties have already been discussed in Paper VI. We confirm the separation at $\log P \sim -0.1$ between long-period and high-amplitude with short-period and low-amplitude ACs. In passing we note that three out of the 20 ACs have periods around one day, thus further supporting the need for data sets covering large time intervals to remove the one-day alias.

Note that in the current analysis of evolved variables we did not include the six RRLs (three RR_c, three RR_{ab}) and the three ACs recently detected by VM13 outside the tidal radius of Carina. The reasons are the following. The three RR_c variables attain periods that are systematically shorter ($-1.0 \lesssim \log P \lesssim -0.25$) that typical RR_c variables (see Table 7), but their mean $B - V$ colors are typical of RR_{ab} variables. The same outcome applies to the three RR_{ab} variable, and indeed they are located in the short period range of fundamental pulsators, but their $B - V$ colors are typical of objects located close to the red edge of the IS. Moreover, the newly identified ACs have periods that are systematically shorter ($-0.8 \lesssim \log P \lesssim -0.7$) than the typical Carina ACs.

3.2. Petersen Diagram

The top panel of Figure 7 displays the position of the Carina RR_d variables in the Petersen diagram, i.e., the first-overtone-to-fundamental period ratio (P_1/P_0) versus the fundamental period. The data in this panel also show the comparison with

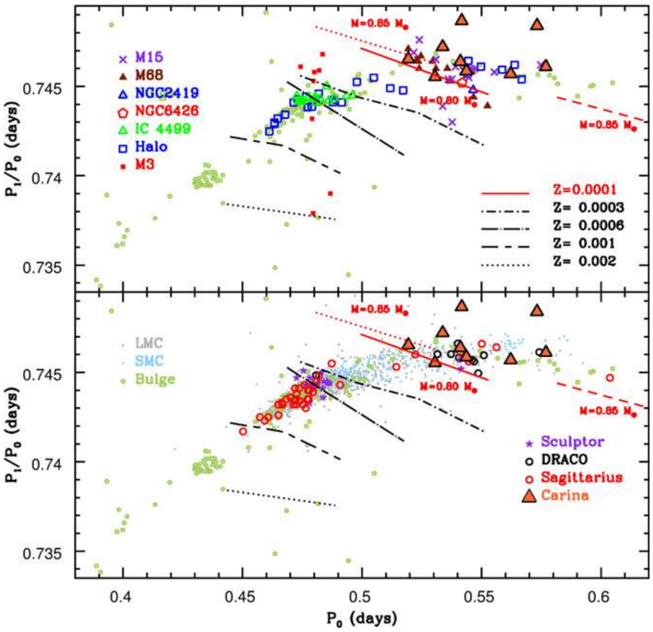

Figure 7. Top: comparison in the Petersen diagram between Galactic (halo, bulge, globular clusters), and Carina (orange triangles) RR_d variables. Pulsation predictions (M2015) for different chemical compositions (see the labeled values) are plotted with different lines. The stellar mass of the pulsation models for the most metal-poor chemical composition are also labeled. Bottom: same as the top, but the comparison is with RR_d variables in nearby dwarf spheroidals and irregulars. The RR_d of the Galactic bulge are also plotted.

RR_d variables identified in Galactic globulars (see labeled names) and in the Galactic field (Halo: blue squares; Bulge: small green circles). Table 8 gives from left to right the name of the stellar system, the number of RR_d variables, the reference for the RR_d data, the mean metallicity, and the reference for the metallicity estimate. The data plotted in this figure display several interesting features.

The period ratio shows a steady decrease when moving from more metal-poor to more metal-rich systems (see also Bragaglia et al. 2001). The largest values in the period ratio are attained in the Halo and in very metal-poor GCs, while the smallest values are attained in the Bulge. The trend with the metallicity was also suggested on both theoretical and empirical bases by Soszyński et al. (2011) and more recently by Soszyński et al. (2014). Note that the fraction of double-mode variables appears to be anti-correlated with the mean metal abundance, and indeed it increases from 0.5% in the Bulge to 4% in the LMC and to 10% in the SMC (Soszyński et al. 2011). The RR_d variables in Carina appear to follow a similar trend, since the current fraction is ~10%. Two RR_d variables (V192, V210) display period ratios that are systematically larger then period ratios in Galactic globulars, in dwarf galaxies, and in the Bulge. In passing we note that one RR_d in M68 (V36) and two in M15 (V51, V53) display period ratios that systematically smaller than the bulk of RR_d variables. The referee suggested the difference on a more quantitative basis. To avoid spurious fluctuations in the period range covered by the different data sets, we ranked the entire sample (398) as a function of the fundamental period. Then we estimated the running average by using a box including the first 40 objects in the list. We estimated the mean period ratio, the mean fundamental period, and the standard deviations of this subsample. We estimated the same quantities by moving one object in the ranked list until we took account of the last 40 objects in the sample. We performed several tests, changing both the number of objects included in the box and the number of stepping stars. The current findings are minimally affected by plausible variations. We found that the quoted five RR_dstars are located within 3σ of the mean. The current statistics is too limited to claim solid evidence of discrepancy. Note that we double checked the photometric quality and coverage of the above five objects and we found that they are similar to the other canonical RR_dstars.

The period ratios display a larger spread when moving into the metal-poor regime (long fundamental periods). To define the trend on a more quantitative basis we adopted several sets of nonlinear, convective pulsation models (M2015). The adopted chemical compositions are labeled. The new set of RRL models relies on the theoretical framework outlined in Di Criscienzo et al. (2004) and Marconi et al. (2011), but on new evolutionary prescriptions for low-mass He burning models provided by (Pietrinferni et al. 2004) (BASTI data base, http://albione.oa-teramo.inaf.it). The pulsation predictions plotted in this panel cover the so-called OR region, i.e., the region in which RRLs show a stable limit cycle in both the fundamental and the first overtone mode. This region is located between the blue edge of the fundamental mode and the red edge of the first overtone. The comparison between theory and observations indicates that an increase in the luminosity ($\log L/L_\odot = 1.76$, 1.86, dotted and dashed red lines) mainly causes, at fixed chemical composition ($Z = 0.0001$) and stellar mass ($M/M_\odot = 0.85$), a steady increase in the fundamental period, and in turn a decrease in the period ratio. Moreover, a decrease in stellar mass ($M/M_\odot = 0.80$, solid red line) at fixed chemical composition and luminosity level ($\log L/L_\odot = 1.76$) causes a systematic decrease in the period ratio and a moderate increase of the fundamental period. The above trends take into account a significant fraction of RR_d pulsators located in metal-poor GCs and in Carina dSph. This indicates that RR_d in Carina have a metallicity of the order of $Z = 0.0001$ and a mean stellar mass close to 0.85 $M_\odot$. The pulsation masses are slightly larger than predicted by evolutionary models, but are within the current empirical and theoretical uncertainties.

The above findings further support the evidence that the old stellar component in Carina is quite metal-poor. This evidence is soundly supported by recent photometric and spectroscopic results by Monelli et al. (2014) and Fabrizio et al. (2015) suggesting a mean metal abundance for the old stellar component of $[Fe/H] = (-2.13 \pm 0.03 \pm 0.28)$ dex.

In this context it is worth mentioning that theoretical predictions for more metal-rich pulsation models (see the black lines and the labeled values) provide a sound explanation of the steady decrease in the period ratio of Bulge RR_d variables, i.e., the stellar systems with the broader metallicity distribution.

To further define the pulsation and evolutionary properties of Carina RR_d variables, the bottom panel of Figure 7 shows the same Petersen diagram, but the comparison is now extended to RR_d in nearby dwarf spheroidals (Draco, Sculptor, Sagittarius), in dwarf irregulars (LMC; Small Magellanic Cloud, SMC) and in the Bulge. The data plotted in this panel bring forward several interesting new findings.

The range in period ratios covered by LMC RR_d is on average larger ($0.740 \leqslant P_1/P_0 \leqslant 0.749$) than the range of SMC RR_d variables. This evidence supports spectroscopic

Table 8
Number of RR_d Hosted in the Stellar Systems Plotted in Figure 7 and Their References

System	N	Reference	[Fe/H]	Reference
NGC 2419	1	Clement et al. (1993)	−2.20 ± 0.09	Carretta et al. (2009)
NGC 6426	1	Clement et al. (1993)	−2.33 ± 0.15	Hatzidimitriou et al. (1999)
LMC	985	Soszyński et al. (2009)	−0.33 ± 0.13	Romaniello et al. (2008)[a]
SMC	257	Soszyñski et al. (2010)	−0.75 ± 0.08	Romaniello et al. (2008)[a]
Bulge	173	Soszyński et al. (2014)	−1.5/–0.5	Zoccali et al. (2008)[b]
Halo (NSV 09295)	1	Garcia-Melendo & Clement (1997)	−1.5	Layden (1994)
Halo (AQ Leo)	1	Clement et al. (1991)	−1.5	Layden (1994)
Halo (VIII–10, VIII–58)	2	Clement et al. (1993)	−1.5	Layden (1994)
Halo (CU Com)	1	Clementini et al. (2000)	−1.5	Layden (1994)
Halo (ASAS)	32	Pojmanski (2002)	−1.5	Layden (1994)
M3	8	Clementini et al. (2004)	−1.50 ± 0.05	Carretta et al. (2009)
IC4499	16	Walker & Nemec (1996)	−1.62 ± 0.09	Carretta et al. (2009)
M68	12	Walker (1994)	−2.27 ± 0.04	Carretta et al. (2009)
M15	14	Nemec (1985b)	−2.33 ± 0.02	Carretta et al. (2009)
Draco	10	Nemec (1985a)	−1.98 ± 0.01	Kirby et al. (2013)
Sculptor	18	Kovács (2001)	−1.68 ± 0.01	Kirby et al. (2013)
Sagittarius	40	Cseresnjes (2001)	−0.62 ± 0.2	Carretta et al. (2010)

Notes. Columns 4 and 5 give the iron abundances of the hosting stellar system and their references.
[a] Mean iron abundances and standard deviations of classical Cepheids based on high spectral resolution spectra. Metal abundances for 98 LMC RRLs were provided by Gratton et al. (2004) using low-resolution spectra and found [Fe/H] = −1.48 ± 0.03 ± 0.06. Metal abundances for SMC RRLs are not available. The iron abundance of the single SMC GC (NGC 121) is [Fe/H] = −1.19 ± 0.12 provided by Da Costa & Hatzidimitriou (1998).
[b] Range in iron abundance covered by red giants in the Galactic bulge. The iron abundance of Bulge RRLs was provided by Walker & Terndrup (1991) [Fe/H] = −1.00 ± 0.16 using low-resolution spectra.

measurements of LMC RRLs suggesting metal abundances ranging from [Fe/H] = −2.12 to −0.27 dex (Gratton et al. 2004). The SMC RR_d cover a slightly narrower period ratio range ($0.741 \leqslant P_1/P_0 \leqslant 0.747$ days) but according to recent studies, and within current uncertainties affecting metallicity estimates for RRLs in these systems (Haschke et al. 2012) the metallicity spread for the old stellar populations in the two Clouds is similar.

The location of RR_d of Carina and Draco is the same in the Petersen diagram. Indeed current spectroscopic estimates, based on medium resolution spectra, provide a very metal-poor iron abundance ([Fe/H] = −1.92 ± 0.01 dex, see Table 8) also for Draco. The steady decrease in period ratio of RR_d in Sculptor is strongly supported by the recent spectroscopic measurements suggesting an iron abundance of [Fe/H] = −1.68 ± 0.01 dex (see Table 8). The empirical evidence concerning Sagittarius needs to be discussed in detail, because the periods and period ratios attain values that are on average smaller than for RR_d in other dSphs. Spectroscopic estimates based on high-resolution spectra by Carretta et al. (2010), suggest for Sagittarius a mean iron abundance, based on 27 RGs, of [Fe/H] = −0.62 and individual values ranging from −1.0 to above solar. A smaller spread in iron abundance was also suggested by (Kunder & Chaboyer 2008) using RR Lyrae properties. The spread in period ratios and the range in fundamental periods ($0.45 \leqslant P \leqslant 0.49$ days) showed by Sagittarius RRLs soundly support the spectroscopic measurements and the similarity with LMC RRLs. This indicates that Sagittarius is a fundamental nearby laboratory to constrain the pulsation properties of metal-rich RRL in gas poor systems.

The RR_d in the Bulge (small green circles) display a clear overdensity for $P_0 \sim 0.46$ days. This overdensity was explained by Soszyński et al. (2011) as the relic of a former dwarf galaxy that was captured by the Milky Way. More recent investigations based on a larger sample (28 versus 16) indicate that they are distributed along a stream that crosses the Galactic bulge almost vertically. Note that the comparison with theoretical predictions suggests, for the above stellar system, a metal-intermediate chemical composition (Z = 0.001–0.002).

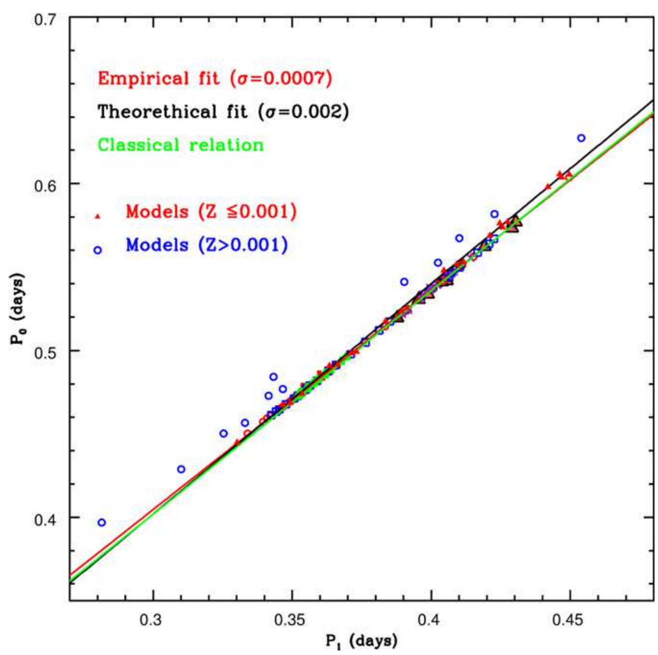

Figure 8. Correlation between fundamental and first overtone periods. Observed RR_d variables have been plotted using the same symbols of Figure 7. The red line shows the fit to the observed data, the black line shows the fit to the pulsation models and the green line shows the classical relation. Red triangles and blue dots display metal-poor and metal-rich pulsation models.

The RR_d also provide a unique opportunity to validate the current approach to fundamentalizing the first overtones. Whenever the sample of RRLs hosted in a stellar system is limited, fundamental and first overtone variables are treated as

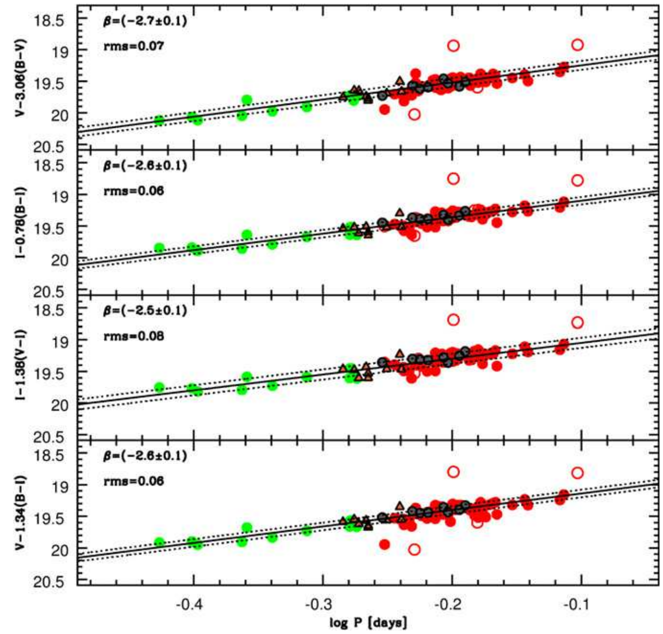

Figure 9. Observed optical PW relations. From top to bottom the different panels display the *BV*, the *BI*, the *VI*, and the *BVI* relations. First overtone pulsators were fundamentalized. The symbols are the same as in Figure 1. The solid lines display the fit, while the dotted lines show the 1σ difference. The standard deviations (rms), the coefficient of the logarithmic period, and their errors are also labeled. The two empty circles were not included in the estimate of the PW relations.

a single sample by transforming the periods of the first overtones into "equivalent" fundamental periods, using the relation $\log P_{\rm F} = \log P_{\rm FO} + 0.127$. This assumption dates back to almost half a century and relies on the few RR$_d$ variables known at that time (Sandage et al. 1981; Cox et al. 1983; Petersen 1991). The above constant period shift is further supported by the new theoretical scenario by M2015 and by the sizable sample of RR$_d$ variables recently identified by large, dedicated photometric surveys.

In passing we note that this issue is far from being an academic dispute, since the same fix is also used to improve the precision of distance determinations based on both RRLs (Braga et al. 2015) and classical Cepheids (e.g., Marengo et al. 2010). Figure 8 shows fundamental versus first overtone periods (P_0 versus P_1) for the entire sample of RR$_d$ plotted in Figure 7. The red line shows the fit to the empirical data. We found:

$$P_0 = 0.0096 + 1.317 * P_1. \quad (1)$$

The new estimate of both the slope and the zero-point soundly supports the old fix, and indeed the green line, showing the classical fix, agrees quite well with the new observations.

To further constrain the impact that the period ratios of RR$_d$ variables have in constraining the pulsation properties of RRLs, we plotted in the same plane theoretical predictions for the "OR" regions adopted in Figure 7. The black solid line was estimated by considering only models more metal-poor than $Z = 0.001$, i.e., a metallicity range similar to the observed one. The agreement is quite good over the period range. In passing we also note that when moving to more metal-rich models ($Z > 0.001$, blue circles) the period increase is significantly larger in the fundamental period than in the first overtone one.

Table 9
Results of the Empirical Fit of Period–Wesenheit Relations $W = \alpha + \beta \log P_{\rm F}$

α	β	rms
	$W(B, V) = M_V - 3.06(B - V)$	
(18.98 ± 0.03)	(−2.7 ± 0.1)	0.07
	$W(B, I) = M_I - 0.78(B - I)$	
(18.84 ± 0.03)	(−2.6 ± 0.1)	0.06
	$W(V, I) = M_I - 1.38(V - I)$	
(18.80 ± 0.03)	(−2.5 ± 0.1)	0.08
	$W(V, BI) = M_V - 1.34(B - I)$	
(18.88 ± 0.03)	(−2.6 ± 0.1)	0.06

We still lack firm empirical evidence for such objects and it is not clear whether it is an observational bias or the consequence of an evolutionary property connected to the dependence of the HB morphology on the metal content.

4. DISTANCE TO CARINA FROM OPTICAL PERIOD–WESENHEIT RELATIONS

4.1. Carina Distance Determination Based on the Empirical PW BV Relation

One of the most important tools for deriving distances from pulsating stars is the so called Wesenheit relation (see for example, van den Bergh 1975; Madore 1982) that is independent of reddening by definition, assuming that the ratio of total-to-selective absorption is fixed. This is a period–luminosity relation that includes a color term whose coefficient is the ratio between the total and the selective extinction coefficients. Figure 9 shows the observed PW relations and the empirical fit to the data (solid black lines) obtained by fundamentalizing the first overtone pulsators by using Equation (1). Dashed lines depict the dispersion of the above inferred relations. Results of these fits are listed in Table 9, where the zero-points, the slopes, and the dispersions of the relations are reported in the first three columns, respectively. In the fit determination we excluded stars outside 3σ of the inferred empirical *BV* Wesenheit relation. These stars are the two peculiar pulsators V158 and V182 and the stars V170 and V171 for which we have uncertain parameters (red open symbols).

Thanks to the use of the Fine Guidance Sensor on board the *Hubble Space Telescope* (*HST*), Benedict et al. (2011) provided accurate estimates of the trigonometric parallaxes for five field RRLs: SU Dra, XZ Cyg, RZ Cep, XZ Cyg, and RR Lyr. Using their data in Table 2, we derived the mean magnitude in the *B* and *V* bands from a fit with a spline under tension. We then calculated the absolute Wesenheit parameter for each star, ($W = \langle V \rangle - 3.06(B - V) - \mu$), where μ is the individual distance modulus based on the *HST* parallax. Individual mean magnitudes of the calibrating RRLs and their distances are listed in Table 10. We applied the individual calibrating RRL to the empirical PW relations (see Figure 9 and Table 9). Note that the calibrating RRLs cover a limited range in metallicity (from −1.80 to −1.41 dex, Benedict et al. 2011). The current theoretical predictions (see Section 4.2) suggest a mild dependence on the metal content. Therefore, we neglected the metallicity dependence of the calibrating RRLs. The data

Table 10
Periods, *B* and *V* Mean Magnitudes, True Distance Moduli and Metallicity for the Five Field RRLs Stars by Benedict et al. (2011)

Name	log *P*	⟨*B*⟩	⟨*V*⟩	μ	[Fe/H]
RR Lyr	−0.24655	8.07 ± 0.01	7.75 ± 0.01	7.14 ± 0.07	−1.41 ± 0.13
SU Dra	−0.18018	10.23 ± 0.01	9.95 ± 0.01	9.35 ± 0.24	−1.80 ± 0.2
UV Oct	−0.26552	9.71 ± 0.01	9.35 ± 0.01	8.87 ± 0.13	−1.47 ± 0.11
XZ Cyg	−0.33107	10.13 ± 0.01	9.84 ± 0.01	8.98 ± 0.22	−1.44 ± 0.2
RZ Cep	−0.38352	9.92 ± 0.01	9.46 ± 0.01	8.03 ± 0.16	−1.77 ± 0.2

Note. The distance moduli in this column are slightly different than those in Table 8 of Benedict et al. (2011) due to typographical errors in the paper. Iron abundances are on the Zinn & West (1984) metallicity scale according to Benedict et al. (2011; see their Table 1).

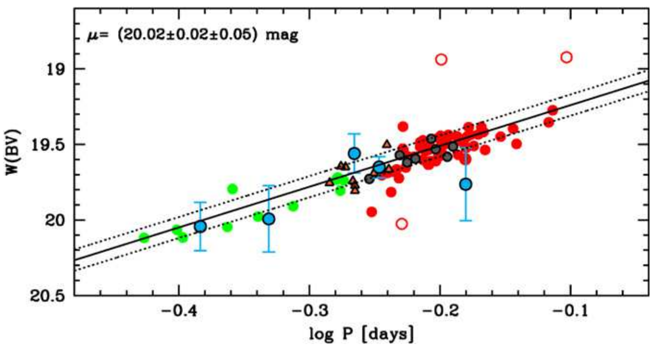

Figure 10. Same as the top panel of Figure 9, but with the the five field RRLs (light blue circles) for which trigonometric parallaxes have been estimated using FGS at *HST*. The vertical error bars take account of the photometric error and of the uncertainty in distance. The object with the smallest error bar is RR Lyr itself. The true distance modulus based on the empirical slope and on the calibrating RRL is labeled.

plotted in Figure 10 show in the W-log *P* plane the calibrating RRLs together with the Carina RRLs. The error bars of the calibrating RRLs take into account both the photometric errors and the uncertainties of the trigonometric parallaxes. A glance at the data discloses that only for RR Lyr is the precision of the absolute distance better than 1%. Using all the calibrating RRLs we found a true distance modulus for Carina of $\mu = (20.02 \pm 0.02 \pm 0.05)$ mag. Note that for the above reasons the accuracy of the distance mainly depends on the accuracy of the data for RR Lyr.

4.2. Carina Distance Determination Based on Theoretical PWZ Relations

To fully exploit the multiband photometry of Carina RRLs we also decided to use predicted PW relations. The new theoretical framework derived by M2015 indicates that the PW (*BV*) relation is independent of the metal content. This is a very positive feature for two different reasons: (a) the PW (*BV*) can be applied to estimate individual distances of field RRLs for which the metal content is not available; (b) the PW (*BV*) is particularly useful to estimate distances of RRLs in nearby dwarf galaxies, since they typically cover a broad range in iron content. We applied the predicted relation to Carina RRLs and we found a true distance modulus of $\mu = (20.08 \pm 0.007 \pm 0.07)$ mag. The distance determination has been estimated using the predicted relation for fundamental pulsators. The number of RR$_c$ variables in Carina is modest (12) and they have been fundamentalized. As noted in the previous section in the current distance determination we did not consider stars outside 3σ of the inferred empirical Wesenheit (*BV*) relation. The above distance agrees, within the errors, quite well with the true Carina distance based on empirical calibrators. Moreover, the new distance determination also agrees with Carina distances available in the literature that are based on robust standard candles (see Table 11).

Table 11
Carina True Distance Moduli Based on Different Diagnostics

μ	*E*(*B* − *V*)	Method	Reference
20.06 ± 0.12	0.025	PL (DC)	Mateo et al. (1998)
20.10 ± 0.12	0.03	PLC	D03
20.00 ± 0.10	0.03	PLA	D03
20.10 ± 0.04	0.03	FOBE	D03
20.11 ± 0.13	0.06	TRGB	Pietrzyński et al. (2009)
20.17 ± 0.10	0.063	PL (DC)	Vivas & Mateo (2013)
20.09 ± 0.07	0.03	PLW	Paper VI

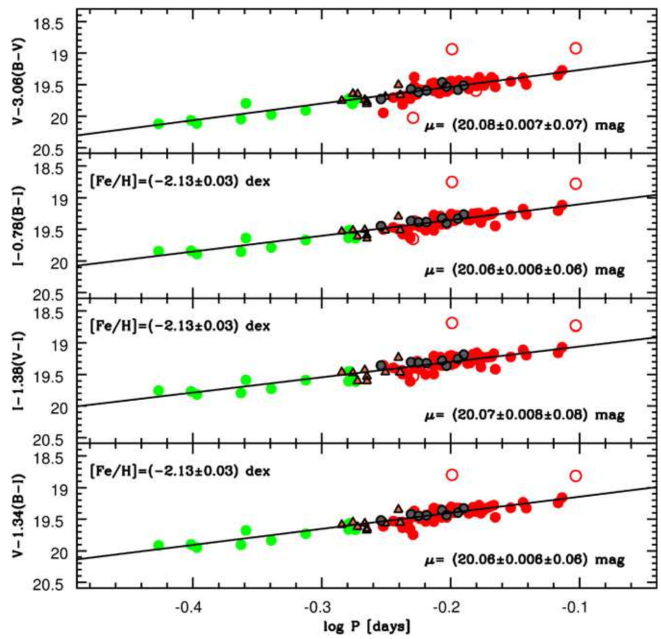

Figure 11. Top: predicted PW (*BV*) relation (black line). The true distance modulus, the standard error of the mean and the standard deviations are labeled. Note that this PW relation is independent of the metal content. Middle: same as the top, but for the PW (*BI*) relation. The true distance modulus was estimated using the labeled value of iron abundance. Bottom: same as the middle, but for the PW (*VI*) relation.

To take advantage of the multiband photometry for Carina RRLs, we estimated the distance using the PWZ (*BI*), the PWZ (*VI*), and the triple band PWZ (*BIV*) relations (see Figure 11). The current pulsation predictions suggest a mild dependence on the metal content. Indeed, the coefficients of the metallicity term are 0.106 (*BI*), 0.150 (*VI*), and 0.075 (*BVI*). In passing we

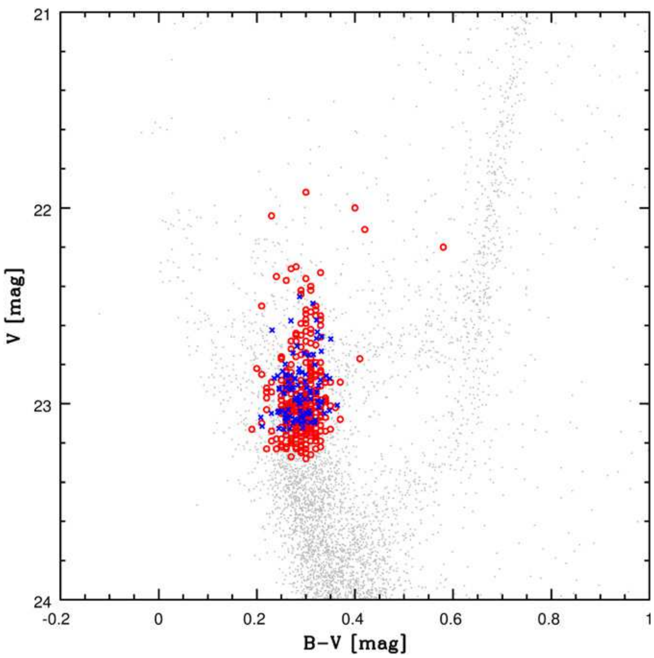

Figure 12. Position of SX Phe in V, $(B-V)$ CMD. Red circles and blue crosses display the VM13 and the new discovered variables, respectively. Their positions, periods, and magnitudes are given in Tables 13 and 12.

note that the metallicity dependence of the optical PW relation for RRL stars displays a different trend when compared with similar relations for classical Cepheids. For the latter objects the PW (VI) relation is almost independent of the metallicity, while the PW (BV) shows a strong dependence on the iron content. The reader interested in a detailed discussion of the difference between RRLs and classical Cepheids is referred to the recent paper by M2015.

To estimate the distance from the PWZ (BI), the PWZ (VI) and the PWZ (BVI) we adopted a mean iron abundance for Carina RRLs of $(-2.13 \pm 0.03 \pm 0.28)$ dex (Fabrizio et al. 2015). Using this value we found the following true distance moduli: $\mu = (20.086 \pm 0.006 \pm 0.06)$ mag (BI), $\mu = (20.07 \pm 0.008 \pm 0.08)$ mag (VI), and $\mu = (20.06 \pm 0.006 \pm 0.06)$ mag (VBI). Note that the uncertainties in the distance modulus account for the photometric errors, the standard deviation of the theoretical PWZ relations and the intrinsic spread in iron abundance. Once again the above distance determinations agree quite well with the empirical distance, with the distance based on the PW (BV), and with distances available in the literature.

5. SX PHOENICIS

More that 30 years ago Niss (1981) identified the first variable Blue Straggler (BS) in the Galactic globular ω Cen. The oscillating BSs have been the cross-road of several theoretical (Gilliland et al. 1998; Santolamazza et al. 2001; Fiorentino et al. 2015b) and observational (Kaluzny & Thompson 2003; Olech et al. 2005; Fiorentino et al. 2014) investigations. However, no general consensus has been reached yet on their evolutionary and pulsation properties. The names suggested in the literature range from SX Phoenicis (Nemec & Mateo 1990, p. 134) to Dwarf Cepheids (Mateo et al. 1998; Vivas & Mateo 2013) to ultra-short-period Cepheids (Eggen 1979) to AI Velorum stars (Bessell 1969) to high-amplitude δ Scuti stars (McNamara 1995; Hog & Petersen 1997).

The most relevant point concerning the classification is that SX Phe are considered the metal-poor extension of the classical δ Scuti stars. Ironically, the prototype, SX Phe itself, is a metal-intermediate ([Fe/H] $= -1.3$ dex; Hog & Petersen 1997). The circumstantial empirical evidence concerning the pulsation properties are: they oscillate both in radial and non radial modes and a significant fraction are mixed-mode variables (Gilliland et al. 1998); their amplitude ranges from a few hundredths to a few tenths of magnitude; they do not show a clear separation in the Bailey diagram (luminosity amplitude versus pulsation period), this means that the mode identification based on their pulsation properties is not trivial; they obey a period–luminosity (McNamara 2000) and a period–luminosity–color–metallicity (Petersen & Christensen-Dalsgaard 1999; Fiorentino et al. 2013).

The region of the CMD in which these objects are located is strongly affected by degeneracy. They are at the transition between low- and intermediate-mass stars during either central hydrogen burning or thick shell hydrogen burning. However, the same region is also crossed by stellar structures approaching the main sequence (Marconi et al. 2000) and by stellar structures that experienced either a collisional merging or a binary merging, i.e., the so-called BSs (Dalessandro et al. 2013).

The above evidence indicates that the evolutionary channel producing field δ Scuti and SX Phe can hardly be constrained by their position in the CMD or the Bailey diagram. The empirical scenario becomes easier for variables hosted either in open or in globular clusters, since they are typically brighter and bluer than MS turn-off stars. This further supports their "peculiar" evolutionary origin.

In this context, dwarf galaxies play a crucial role. The stellar content of dwarf spheroidal galaxies that experienced only a single star formation event (Cetus Monelli et al. 2012a) and (Tucana Monelli et al. 2010a) appears similar to globular clusters. These stellar systems are dominated by old ($t > 10$ Gyr) stellar populations, therefore the colors of their main sequence turn off stars (MSTO) are systematically redder (cooler) than the red edge of the IS. This means that the Cepheid IS in these stellar systems can only be crossed by BSs, since these objects are hotter and brighter than canonical MSTO stars. However, dwarf galaxies that underwent multiple star formation episodes, in particular a well defined star formation episode 6–9 Gyrs ago, are going to have both "canonical" and "peculiar" objects crossing the Cepheid IS. The Carina dwarf spheroidal galaxy belongs to the latter group.

The above scenario has been soundly supported by the recent detailed photometric investigation by VM13. They identified more than 340 new SX Phe in Carina with periods ranging from 0.03860 to 0.18058 days and luminosity amplitudes ranging from 0.22 to 1.10 mag in the V band. In this context it is worth mentioning that their magnitude ($21.89 \leqslant V \leqslant 23.55$) and color distribution ($0.05 \leqslant B-V \leqslant 0.54$) indicate that only a minor fraction belongs to the so-called Blue Plume ($22.0 \leqslant V \leqslant 23.2$; $0.02 \leqslant B-V \leqslant 0.22$), i.e., to the objects for which it is not clear whether they are truly young ($t < 1$ Gyr) or BSs of the old populations (Okamoto et al. 2008; Monelli et al. 2012b). The bulk seem to belong to canonical main sequence intermediate-age stars. This evidence opens a new path in the investigation of these interesting objects, since we are dealing with objects that are the aftermath of the different channels located at the same distance and covering a narrow range in metal abundances (Fabrizio et al. 2015).

Although, the investigation by VM13 is a substantial step forward in the identification of these objects we decided to further investigate the possible occurrence of SX Phe stars. The working hypothesis was mainly supported by the slope of the Cepheid IS suggesting that the actual sample of SX Phe might be even larger. The similarity of the Cepheid IS with the location of SX Phe, δ Scuti, and RR Lyrae stars is supported by detailed investigations concerning their pulsation properties (McNamara 2011; McNamara & Barnes 2014). Thanks to the photometric precision and accuracy of our multiband photometric catalog we identified 101 new SX Phe. Some examples of light curves are plotted in Figure set 3, while their positions, epochs, periods and mean magnitudes are listed in Table 12. Finally, Figure 12 shows the position of VM13 (red circles) and the new discovered (blue crosses) SX Phe in *IV* (B–V) CMD. The mean magnitudes were estimated as intensity means using an analytical fit of the light curves. Moreover, we confirm the variability for 324 out of the 340 known SX Phe in Carina. For the other 16, we have insufficient data for DC-1, DC-2, DC-3, DC-4, DC-5, DC-6, DC-284, and DC-339, and we do not confirm the variability for DC-75, DC-158, DC-264, and DC-295, we do not find DC-180 and DC-340 and we consider DC-1, DC-111 and DC-144 the same variable. The pulsation properties for these objects are given in Table 13.

The comparison between predicted and observed evolutionary and pulsation properties of Carina SX Phe will be discussed in a forthcoming paper.

6. CONCLUSIONS AND FUTURE PERSPECTIVES

We have discussed new and accurate multiband optical (*UBVI*) photometry of helium burning variables in the Carina dwarf spheroidal galaxy. The current photometry covers a time interval of more than 20 years. This means that we can provide robust identification of regular variables with periods close to a half and one day, as well as variables showing modulations in the pulsation period and/or in in amplitude (mixed mode pulsators, Blazhko).

We ended up with a sample of 92 RRLs, among them 12 first overtones (RR_c), 63 fundamental (RR_{ab}) pulsators, 9 mixed-mode variables (RR_d), and 8 candidate Blazhko variables (Bl). Six out of the 92 RRL variables are new identifications. Moreover, we identified one new double mode pulsator. We also identified 20 ACs, and among them 1 is a new identification. Together with all these variables we found two new LPVs and seven EB candidates.

For the entire sample of variables we provide accurate pulsation properties (periods, luminosity amplitudes) plus accurate estimates of the mean *BVI* magnitudes. The mean *BV* magnitudes are based on a spline fit, while the mean *I*-band mean magnitude is based on a template fit. For the RR_d variables we have been able to estimate the two oscillating frequencies and also the luminosity amplitude of both the FO and the F component. The current data do not allow us to constrain the secondary oscillation of the candidate Blazhko RRLs. According to extensive photometric surveys of field RRLs, they are a minor fraction (8%) of Blazhko RRLs (Soszyński et al. 2011).

Although the pulsation properties of ACs in Carina are very accurate we are still facing the problem of mode identification. It seems that optical bands do not help us in settling this longstanding problem.

The analysis of the Bailey diagram confirms that Carina is an Oosterhoff intermediate system and shows that the luminosity amplitudes of the FO component in RR_d variables are located along the long-period tail of "regular" RR_c variables, while the fundamental components are located along the short-period tale of "regular" RR_{ab} variables. To our knowledge this is the first time that we can properly locate the two components of RR_d variables.

The comparison between theory and observations in the Petersen diagram for RR_d variables indicates that a steady increase in the metal content causes a steady decrease in the period ratio and in the fundamental period. This evidence is supported not only by RR_d variables in Galactic globulars, but also by RR_d variables in the Galactic halo and bulge. Moreover, the same diagram shows that RR_d variables in nearby dwarf spheroidals and dwarf irregulars (the Magellanic Clouds) display similar properties and that Carina RR_d variables are located in a region in which there are only RR_d variables hosted in metal-poor globular clusters (M15, M68), in the Halo, or in metal-poor dwarf spheroidal galaxies (e.g., Draco).

The new accurate and precise mean magnitudes allowed us to provide new independent estimates of Carina's true distance modulus. We investigated four different reddening-free Period-Wesenheit relations (*BV*, *BI*, *VI*, *BVI*). We found that the PW (*BV*) is independent of the metal content. This finding soundly supports recent pulsation predictions based on nonlinear, convective, hydrodynamical models of RRL stars (M2015).

We took advantage of the trigonometric parallaxes for five field RRLs provided by Benedict et al. (2011) to give a new independent estimate of Carina's true distance modulus using the observed slope of the PW (*BV*) relation. We found $\mu = 20.02 \pm 0.02$ (standard error of the mean) ± 0.05 (standard deviation) mag. The distance was evaluated using the entire sample of variables. In particular, the RR_c variables were fundamentalized. The above estimate agrees, within the errors, with Carina distances available in the literature that are based on solid standard candles (see Table 11).

To take advantage of the new predicted optical and NIR PW relations provided by M2015 we also estimated the Carina distances using the zero-point and the slope of the PWZ (*BV*, *BI*, *VI*, *BVI*) relations. We found true distance moduli of $\mu = (20.08 \pm 0.007 \pm 0.07)$, $\mu = (20.06 \pm 0.006 \pm 0.06)$, $\mu = (20.07 \pm 0.008 \pm 0.08)$ mag, and $\mu = (20.06 \pm 0.006 \pm 0.06)$ mag. Note that the distances based on both predicted and empirical PW (*BV*) relations are independent of the metal content. The distances based on the PWZ (*BI*, *VI*, *BVI*) relations have been estimated by assuming a mean iron abundance for Carina RRLs of $[Fe/H] = (-2.13 \pm 0.03 \pm 0.28)$ dex. All the above distances are independent of uncertainties in the reddening. However, they rely on the assumption that the reddening law adopted to estimate the color coefficients of the PW relations is appropriate. The true distances based on empirical and predicted PW relations agree quite well with each other and with similar distances available in the literature.

There is evidence that distances based on the theoretical calibrations are ~0.05–0.1 mag larger than the distance based on empirical calibrations. The evidence applies not only to the PW relation that is independent of metallicity, but also to the PW relation based on triple bands indicates that the

Table 12
Pulsation Properties of the New Carina SX Phe

ID	α	δ	Period (day)	$\langle B\rangle^b$	$\langle V\rangle^b$	$\langle I\rangle^b$
341	06 40 14.14	−51 01 23.4	0.05898004	23.11	22.85	22.42
342	06 40 15.46	−51 08 31.2	0.06404925	23.25	22.94	22.50
343	06 40 17.76	−50 56 06.0	0.06189917	22.99	22.70	22.33
344	06 40 23.45	−51 00 18.5	0.05700707	23.39	23.04	22.49
345	06 40 23.84	−50 55 16.0	0.0616327	23.28	23.04	22.65
346	06 40 26.44	−50 55 12.2	0.06983306	23.20	22.93	22.48
347	06 40 34.03	−50 56 36.9	0.06382168	23.17	22.92	22.49
348	06 40 38.49	−50 50 34.2	0.05887662	23.01	22.74	22.34
349	06 40 38.82	−51 13 52.6	0.05220283	23.32	23.03	22.61
350	06 40 40.71	−50 58 29.0	0.05225971	23.12	22.86	22.49
351	06 40 49.07	−50 53 10.6	0.06510992	23.34	23.04	22.62
352	06 40 49.13	−50 54 37.1	0.05555380	22.84	22.58	22.16
353	06 40 49.50	−51 01 26.7	0.05860522	23.17	22.92	22.62
354	06 40 55.07	−50 55 18.3	0.0559396	23.35	23.06	22.65
355	06 40 58.61	−50 55 05.4	0.06195699	23.33	23.07	22.74
356	06 40 59.22	−50 56 52.2	0.05387742	23.26	22.97	22.55
357	06 41 02.69	−50 57 05.9	0.05802369	23.41	23.09	22.66
358	06 41 03.13	−50 51 51.1	0.04853505	23.10	22.86	22.51
359	06 41 02.86	−50 58 00.1	0.05870867	23.29	23.04	22.49
360	06 41 04.51	−50 55 07.3	0.05059894	23.05	22.80	22.41
361	06 41 07.09	−50 47 50.9	0.05405631	23.33	23.07	22.59
362	06 41 06.85	−51 04 14.1	0.05004092	22.89	22.57	22.18
363	06 41 08.60	−50 54 35.8	0.0591939	23.29	23.04	22.67
364	06 41 11.16	−51 00 11.8	0.06534271	23.29	23.00	22.63
365	06 41 12.44	−50 45 31.2	0.05781447	23.33	23.06	22.60
366	06 41 13.10	−51 09 07.4	0.05277468	23.28	23.04	22.64
367	06 41 14.32	−51 01 57.8	0.06230673	23.19	22.90	22.45
368	06 41 14.88	−50 55 16.6	0.07088727	23.21	22.88	22.46
369	06 41 15.33	−50 55 12.5	0.05923093	23.29	23.03	22.63
370	06 41 16.36	−50 54 36.0	0.05263070	23.24	22.97	22.53
371	06 41 18.51	−50 51 48.0	0.0610961	23.14	22.87	22.49
372	06 41 23.09	−51 07 42.1	0.06317447	22.99	22.66	22.28
373	06 41 24.30	−50 59 25.6	0.05712586	23.41	23.10	22.61
374	06 41 24.29	−51 04 21.8	0.05256096	23.02	22.67	22.28
375	06 41 25.07	−50 55 53.9	0.07412219	23.06	22.75	22.33
376	06 41 26.05	−51 12 19.0	0.0739414	23.20	22.86	22.46
377	06 41 28.18	−50 55 26.9	0.05301314	23.06	22.73	22.34
378	06 41 28.80	−50 43 11.2	0.05483068	23.42	23.12	22.71
379	06 41 28.81	−51 00 20.0	0.07092323	23.12	22.80	22.38
380	06 41 29.87	−50 52 05.1	0.06527955	22.99	22.67	22.27
381	06 41 32.44	−50 47 57.3	0.07488229	22.96	22.63	22.19
382	06 41 32.63	−50 57 43.7	0.07197212	23.31	22.98	22.63
383	06 41 32.93	−50 52 54.2	0.1594306	23.28	23.07	22.78
384	06 41 33.43	−50 52 48.5	0.05863985	23.32	22.98	22.49
385	06 41 33.65	−50 57 37.8	0.05633247	22.80	22.49	22.19
386	06 41 35.77	−51 00 39.1	0.0636862	23.20	22.95	22.52
387	06 41 36.96	−50 57 47.0	0.05627784	23.37	23.13	22.73
388	06 41 37.74	−50 55 13.6	0.06400101	23.15	22.85	22.52
389	06 41 37.61	−50 58 58.0	0.07160168	23.06	22.75	22.44
390	06 41 39.58	−50 57 01.2	0.0582159	23.32	22.99	22.60
391	06 41 42.92	−50 52 31.4	0.06104802	23.23	22.91	22.43
392	06 41 44.17	−50 44 22.9	0.06385933	22.74	22.45	21.87
393	06 41 44.84	−51 03 48.3	0.05746218	23.37	23.09	22.72
394	06 41 45.69	−50 50 01.3	0.04855492	23.15	22.89	22.62
395	06 41 49.86	−51 00 21.5	0.05655043	22.86	22.62	22.33
396	06 41 49.87	−51 00 32.4	0.06046970	23.26	22.94	22.55
397	06 41 51.00	−50 58 05.9	0.0645517	23.40	23.09	22.70
398	06 41 51.59	−50 53 05.0	0.06014112	23.39	23.09	22.67
399	06 41 51.66	−50 56 08.9	0.04527754	23.17	22.93	22.58
400	06 41 57.09	−50 55 08.0	0.06364862	23.24	22.95	22.49
401	06 41 58.08	−50 57 58.1	0.05734282	23.12	22.84	22.47
402	06 41 59.28	−51 00 00.0	0.07441239	23.12	22.85	22.39
403	06 41 59.76	−50 55 35.4	0.04671546	23.17	22.90	22.48
404	06 42 00.27	−50 52 19.9	0.06205412	23.28	22.97	22.63

Table 12
(Continued)

ID	α	δ	Period (day)	$\langle B\rangle^b$	$\langle V\rangle^b$	$\langle I\rangle^b$
405	06 42 01.47	−50 52 27.1	0.06348319	23.37	23.01	22.55
406	06 42 01.82	−50 51 30.4	0.06373945	23.04	22.74	22.35
407	06 42 03.52	−50 57 33.5	0.05525245	23.19	22.92	23.19
408	06 42 03.49	−51 01 12.2	0.05567260	23.20	22.95	22.54
409	06 42 05.51	−50 57 43.0	0.05779336	23.38	23.03	22.66
410	06 42 07.77	−51 00 51.5	0.05261781	23.19	22.92	22.45
411	06 42 08.13	−50 52 36.7	0.06459468	23.11	22.82	22.37
412	06 42 09.22	−50 55 36.2	0.05646218	23.27	22.98	22.58
413	06 42 09.61	−51 01 03.4	0.06032828	23.34	23.02	22.54
414	06 42 12.67	−50 56 23.8	0.05842271	23.22	22.87	22.42
415	06 42 13.13	−50 56 01.6	0.05598982	23.18	22.89	22.44
416	06 42 17.19	−50 51 18.2	0.05422022	23.33	23.07	22.63
417	06 42 17.68	−50 48 39.2	0.06434278	23.26	22.98	22.63
418	06 42 19.08	−50 47 46.7	0.05607941	23.22	22.92	22.50
419	06 42 19.88	−50 45 04.8	0.05780775	23.36	23.07	22.50
420	06 42 21.25	−50 45 35.8	0.06575657	23.15	22.87	22.43
421	06 42 22.01	−50 50 06.5	0.05161476	23.36	23.07	22.65
422	06 42 23.24	−50 54 50.4	0.07029254	23.13	22.84	22.23
423	06 42 23.67	−50 49 16.7	0.06527164	23.08	22.83	22.48
424	06 42 24.87	−51 03 02.1	0.07014507	23.22	22.92	22.37
425	06 42 25.71	−50 57 00.4	0.05172937	23.28	23.00	22.53
426	06 42 30.36	−50 49 05.9	0.06320298	23.10	22.87	22.50
427	06 42 31.01	−50 46 02.6	0.05587489	23.38	23.13	22.70
428	06 42 31.58	−50 57 28.1	0.05228718	23.36	23.05	22.65
429	06 42 33.88	−50 48 46.0	0.05360831	23.33	23.11	22.53
430	06 42 33.99	−50 48 03.3	0.05866563	23.39	23.10	22.64
431	06 42 35.21	−50 55 04.0	0.05962675	23.40	23.08	22.66
432	06 42 35.53	−51 02 22.6	0.05995828	23.35	23.05	22.58
433	06 42 37.57	−50 57 41.4	0.05497264	23.37	23.10	22.67
434	06 42 38.39	−50 53 16.7	0.07192960	23.24	22.93	22.43
435	06 42 41.09	−50 49 38.2	0.06649085	23.34	23.04	22.64
436	06 42 42.07	−50 57 31.2	0.05926036	23.39	23.13	22.70
437	06 42 49.56	−50 51 53.9	0.05158018	23.30	23.05	22.70
438	06 42 55.43	−50 54 43.3	0.06550635	23.29	23.00	22.60
439	06 42 55.57	−50 52 55.2	0.06189711	23.35	23.08	22.59
440	06 43 01.04	−50 52 07.7	0.05804751	23.35	23.09	22.70
441	06 43 04.87	−50 53 45.1	0.06346540	23.26	22.98	22.62
442	06 43 25.38	−50 52 26.9	0.05947808	23.28	23.05	22.65

difference is mainly caused by a difference in the zero-point. The comparison between distances based on empirical and on predicted PW relations for stellar systems with precise distances are required to constrain possible systematics either in the current trigonometric parallaxes or in the predicted luminosities at fixed mass.

The above findings further support the mature phase that RRLs are approaching as distance indicators. This circumstantial evidence is going to be reinforced using either NIR and/or MIR PW relations (Madore et al. 2013; Braga et al. 2015). The key advantage of the above findings is that RRL PW relations display either a mild or a vanishing metallicity dependence. This offers a unique opportunity to estimate individual distances for a significant fraction of Halo and Bulge RRLs that have been recently discovered by long-term photometric surveys (OGLE IV, Soszyński et al. 2014; Catalina, Drake et al. 2009; LINEAR, Palaversa et al. 2013; LONEOS, Miceli et al. 2008; ASAS, Pojmanski 2002; QUEST, Vivas et al. 2004; *Gaia*, Eyer et al. 2012). This appears to be a crucial stepping stone before RRLs can be used as solid primary distance indicators in the local universe.

The recent findings concerning the difference in iron and in Mg distribution between the old and the intermediate-age Carina stellar populations opened the path for a more detailed pulsation analysis of Carina SX Phe stars. In a recent investigation Fiorentino et al. (2015b) found that the pulsation properties of SX Phe can provide solid constraints on their pulsation masses. This approach has already been applied to canonical Galactic globulars (NGC 6541, Fiorentino et al. 2014) and to Omega Centauri, i.e., in stellar systems mainly hosting old stellar populations. The sizable sample of Carina SX Phe stars is a very promising laboratory to constrain the mass distribution of the different stellar populations. Moreover, they are located at the same distance, and therefore they offer a unique opportunity to constrain whether the aftermaths of single and binary star evolution display different mass–luminosity relations. This means the prodrome for their use as solid distance indicators.

It is a real pleasure to thank the referee, Mario Mateo, for the positive opinion concerning the content of the paper and for several suggestions and insights that improved the readability and the cut of the paper. This work was partially supported by PRIN–INAF 2011 “Tracing the formation and evolution of the Galactic halo with VST” (PI: M. Marconi) and by PRIN–MIUR (2010LY5N2T) “Chemical and dynamical evolution of the Milky Way and Local Group galaxies” (PI: F. Matteucci). M.

Table 13
Pulsation Properties of the Known Carina SX Phe

ID	α	δ	Period (day)	$\langle B\rangle^b$	$\langle V\rangle^b$	$\langle I\rangle^b$	M98
7	06 39 53.11	−51 04 31.5	0.05861265	23.43	23.13	22.12	…
8	06 39 56.16	−51 06 43.6	0.0840233	22.66	22.36	21.92	…
9	06 40 00.79	−50 57 58.5	0.06283058	23.33	23.04	22.45	…
10	06 40 03.36	−51 07 55.6	0.06600411	23.19	22.93	22.43	…
11	06 40 06.08	−50 55 58.0	0.0566776	23.32	23.04	22.58	…
12	06 40 14.68	−51 05 05.0	0.05116040	23.46	23.18	…	…
13	06 40 17.93	−50 56 33.7	0.0572522	23.27	23.01	22.59	…
14	06 40 18.59	−51 03 01.9	0.05801669	23.33	23.06	22.67	…
15	06 40 21.39	−51 01 02.2	0.06133516	23.14	22.92	22.57	…
16	06 40 23.91	−51 06 44.4	0.06490812	23.16	22.90	22.50	…
17	06 40 27.16	−51 06 17.6	0.06391992	23.31	22.99	22.52	…
18	06 40 27.18	−51 01 03.4	0.06005208	23.36	23.07	22.66	…
19	06 40 28.33	−50 52 58.8	0.05846323	23.16	22.94	22.64	…
20	06 40 29.07	−50 55 58.4	0.05692126	23.28	23.01	22.49	…
21	06 40 31.67	−51 08 54.2	0.07130197	23.12	22.81	22.37	…
22	06 40 32.86	−51 01 43.4	0.05866617	23.27	23.00	22.54	…
23	06 40 35.66	−50 56 48.1	0.05035238	23.51	23.23	22.83	…
24	06 40 37.79	−50 58 11.5	0.05697949	23.30	23.03	22.61	…
25	06 40 38.21	−50 58 04.9	0.05765942	23.31	23.03	22.58	…
26	06 40 38.84	−50 58 39.7	0.05955433	23.28	23.03	22.64	…
27	06 40 39.93	−51 00 32.7	0.06096031	23.28	22.99	22.61	…
28	06 40 40.56	−51 02 30.7	0.06020401	23.08	22.77	22.35	…
29	06 40 41.70	−50 59 10.5	0.05311877	23.11	22.84	22.44	…
30	06 40 45.02	−50 59 29.4	0.06503761	23.02	22.70	22.30	…
31	06 40 45.26	−51 06 18.6	0.06037914	23.35	23.04	22.56	…
32	06 40 46.39	−50 57 53.4	0.05804718	23.26	22.98	22.58	…
33	06 40 46.64	−51 09 37.3	0.05529873	23.38	23.09	22.65	…
34	06 40 46.76	−50 52 17.5	0.05526398	23.29	23.03	22.64	…
35	06 40 47.68	−50 56 44.1	0.06166175	23.26	22.94	22.48	…
36	06 40 48.00	−50 58 33.9	0.05985196	23.17	22.90	22.49	…
37	06 40 48.47	−51 10 55.6	0.05410886	23.36	23.03	22.62	…
38	06 40 48.81	−51 00 41.2	0.05365485	23.32	23.02	22.58	…
39	06 40 50.04	−50 59 24.6	0.05440634	23.28	23.01	22.57	…
40	06 40 50.29	−51 09 31.2	0.05952932	23.24	22.91	22.47	…
41	06 40 50.86	−50 59 28.7	0.06489616	22.82	22.50	22.11	…
42	06 40 51.77	−51 07 16.9	0.05697602	23.18	22.87	22.48	…
43	06 40 53.52	−51 07 14.6	0.06162396	23.25	22.94	22.46	…
44	06 40 54.40	−51 01 28.4	0.06879427	22.27	22.04	21.49	…
45	06 40 55.63	−51 00 43.0	0.05688051	23.39	23.09	22.72	V4
46	06 40 57.65	−50 56 09.5	0.06778138	23.04	22.74	22.26	…
47	06 40 57.88	−51 02 07.9	0.05986604	23.23	22.98	22.48	…
48	06 40 59.18	−50 49 44.3	0.0565391	23.31	23.04	22.74	…
49	06 40 59.27	−50 50 31.6	0.05626531	23.40	23.14	22.69	…
50	06 40 59.31	−50 56 49.1	0.07320810	22.71	22.42	22.00	…
51	06 40 59.92	−50 48 44.6	0.05879641	23.37	23.08	22.50	…
52	06 41 00.18	−51 07 26.7	0.06380392	23.31	23.00	22.55	…
53	06 41 00.50	−50 54 53.6	0.05843550	23.27	22.99	22.51	…
54	06 41 00.89	−51 00 01.1	0.06134829	23.33	23.06	22.64	…
55	06 41 02.48	−51 00 25.8	0.05870253	23.32	23.01	22.65	V5
56	06 41 02.98	−50 58 41.1	0.05851668	23.29	23.00	22.59	V12
57	06 41 03.29	−50 56 14.8	0.05586523	23.31	23.01	22.15	…
58	06 41 03.89	−50 58 44.1	0.05123522	23.54	23.27	22.59	…
59	06 41 05.03	−51 05 15.2	0.06586275	22.88	22.59	22.18	…
60	06 41 05.44	−50 48 27.0	0.05964722	23.32	23.04	22.42	…
61	06 41 05.72	−50 57 44.1	0.06627047	22.84	22.54	22.13	…
62	06 41 06.14	−50 51 51.3	0.04596514	23.45	23.23	…	…
63	06 41 06.37	−50 49 23.2	0.05920742	23.37	23.06	22.53	…
64	06 41 06.61	−51 08 44.1	0.05839355	23.37	23.07	22.64	V10
65	06 41 06.93	−50 59 18.4	0.06264205	23.26	23.00	22.57	…
66	06 41 07.69	−50 52 34.0	0.0525963	23.37	23.10	22.65	…
67	06 41 07.88	−50 56 00.9	0.06022396	23.35	23.06	22.61	V16
68	06 41 08.76	−50 54 27.4	0.06496999	23.15	22.84	22.31	…
69	06 41 09.70	−50 57 37.9	0.05489874	23.33	23.01	22.61	…
70	06 41 11.27	−50 57 41.0	0.05504275	22.94	22.65	22.22	…

Table 13
(Continued)

ID	α	δ	Period (day)	$\langle B\rangle^b$	$\langle V\rangle^b$	$\langle I\rangle^b$	M98
71	06 41 11.73	−51 01 35.5	0.05628829	23.36	23.06	22.69	…
72	06 41 12.00	−50 53 01.6	0.05684917	23.48	23.18	22.68	…
73	06 41 12.06	−50 56 40.2	0.05332273	23.55	23.25	22.79	…
74	06 41 12.44	−50 53 10.8	0.06307089	22.90	22.57	22.09	…
76	06 41 13.33	−50 56 31.5	0.07069207	22.84	22.53	22.06	…
77	06 41 13.43	−50 53 08.2	0.0641156	23.17	22.86	22.48	…
78	06 41 14.31	−50 59 32.8	0.07554039	23.11	22.79	22.41	V9
79	06 41 14.59	−51 02 49.3	0.06153187	23.19	22.93	22.51	…
80	06 41 14.69	−51 08 44.1	0.05600743	23.35	23.09	22.59	…
81	06 41 14.75	−50 59 20.3	0.06095969	22.53	22.11	21.50	…
82	06 41 15.38	−51 08 24.3	0.05954823	22.93	22.60	22.16	…
83	06 41 15.89	−50 55 44.0	0.05754453	23.17	22.92	22.56	V15
84	06 41 16.15	−51 02 56.8	0.06525352	23.25	22.96	22.60	…
85	06 41 16.81	−51 03 55.9	0.06078077	23.26	22.89	21.68	…
86	06 41 16.87	−50 53 05.0	0.06751050	23.00	22.71	22.28	…
87	06 41 16.89	−51 03 45.9	0.06586277	22.88	22.59	22.18	…
88	06 41 17.29	−51 05 26.6	0.05904829	22.87	22.55	22.06	…
89	06 41 17.81	−50 56 01.9	0.05871582	22.99	22.72	22.31	…
90	06 41 18.05	−50 56 40.5	0.06652948	22.59	22.35	22.02	V14
91	06 41 18.09	−51 03 17.0	0.06557268	23.14	22.83	22.39	…
92	06 41 18.13	−50 59 34.1	0.05762093	23.55	23.23	22.80	…
93	06 41 18.2	−50 52 52.5	0.05359279	23.41	23.11	22.69	…
94	06 41 19.06	−50 56 10.9	0.0604939	23.33	23.04	22.54	…
95	06 41 19.67	−51 09 57.5	0.05337312	23.33	22.99	22.52	…
96	06 41 20.01	−50 59 5.9	0.06881335	22.98	22.68	22.29	…
97	06 41 20.42	−50 59 40.7	0.06044260	23.24	22.89	22.45	…
98	06 41 20.9	−50 58 3.0	0.05979826	23.32	23.04	22.48	…
99	06 41 21.19	−51 02 6.5	0.06289669	23.26	22.99	22.53	…
100	06 41 21.42	−50 57 13.2	0.05890563	23.43	23.13	22.79	…
101	06 41 21.56	−51 00 41.5	0.05224501	23.42	23.12	22.77	…
102	06 41 21.92	−50 57 7.7	0.05272663	23.31	23.04	22.70	…
103	06 41 22.15	−50 57 13.5	0.05679868	22.87	22.57	22.19	…
104	06 41 22.26	−50 57 9.4	0.05467434	23.17	22.90	22.48	…
105	06 41 22.36	−50 58 56.5	0.0604251	23.33	23.07	22.71	…
106	06 41 22.62	−50 51 48.9	0.07006015	22.84	22.53	22.07	…
107	06 41 23.17	−51 01 54.1	0.06589533	23.21	22.91	22.49	…
108	06 41 23.31	−51 01 7.3	0.06002635	23.39	23.12	22.69	…
109	06 41 23.56	−50 53 55.7	0.06008917	23.36	23.05	22.60	…
110	06 41 23.56	−51 02 56.0	0.05742446	23.43	23.14	22.76	…
112	06 41 25.16	−50 42 27.2	0.05093029	23.02	22.77	22.23	…
113	06 41 25.22	−50 58 20.6	0.05366079	23.37	23.10	22.57	…
114	06 41 25.47	−51 00 12.5	0.06051002	22.58	22.31	21.93	…
115	06 41 26.0	−51 03 26.0	0.06565715	23.38	23.10	22.63	…
116	06 41 26.02	−51 06 5.0	0.05160868	23.48	23.16	22.83	…
117	06 41 26.17	−51 07 16.5	0.05743431	23.52	23.19	22.82	…
118	06 41 26.34	−50 57 43.9	0.05157820	23.54	23.25	22.76	…
119	06 41 26.39	−50 56 20.9	0.05193595	23.50	23.19	22.80	…
120	06 41 26.67	−50 58 21.6	0.06033252	23.04	22.75	22.37	…
121	06 41 27.07	−50 53 0.9	0.05577754	23.29	23.02	22.58	…
122	06 41 27.8	−51 01 26.0	0.04680622	23.19	22.89	22.45	…
123	06 41 27.8	−50 59 1.0	0.05847475	23.44	23.15	22.67	…
124	06 41 27.83	−50 55 41.8	0.05863472	23.21	22.87	22.48	…
125	06 41 28.21	−50 53 37.1	0.05675304	23.17	22.84	22.38	…
126	06 41 28.45	−50 59 8.5	0.06369570	23.10	22.84	22.51	…
127	06 41 28.71	−50 58 11.1	0.0601055	23.39	23.06	22.69	…
128	06 41 28.8	−50 51 35.4	0.0527838	23.31	23.04	22.63	…
129	06 41 29.04	−50 53 19.0	0.0544041	23.35	23.08	22.51	…
130	06 41 29.21	−51 00 23.5	0.05956936	22.84	22.52	22.07	…
131	06 41 29.35	−50 55 44.1	0.06545531	23.25	22.96	22.46	…
132	06 41 29.44	−50 57 39.1	0.06719052	23.25	22.96	22.56	V13
133	06 41 29.67	−50 53 14.4	0.05464765	23.39	23.11	22.61	…
134	06 41 29.85	−51 02 34.7	0.05504185	23.44	23.14	22.71	…
135	06 41 29.87	−50 59 37.8	0.0534139	23.49	23.17	22.69	…
136	06 41 30.25	−51 09 3.2	0.04970627	23.40	23.10	22.54	…

Table 13
(Continued)

ID	α	δ	Period (day)	$\langle B\rangle^b$	$\langle V\rangle^b$	$\langle I\rangle^b$	M98
137	06 41 30.42	−50 51 29.1	0.0529662	23.36	23.10	22.72	…
138	06 41 30.47	−50 48 15.3	0.05815515	23.41	23.09	…	…
139	06 41 30.79	−50 55 23.3	0.0644954	23.26	22.94	22.52	…
140	06 41 30.97	−51 06 27.7	0.05051116	23.45	23.08	…	…
141	06 41 32.25	−51 02 38.5	0.05788590	23.48	23.14	22.76	…
142	06 41 32.56	−51 00 56.0	0.06607394	23.31	22.97	22.52	…
143	06 41 32.68	−50 52 58.7	0.06626448	23.27	22.97	22.55	…
145	06 41 32.88	−50 57 21.9	0.05559422	23.30	23.05	22.53	…
146	06 41 33.29	−50 55 52.0	0.05518256	23.42	23.14	22.64	…
147	06 41 33.31	−50 56 21.0	0.0516737	23.27	22.97	22.51	…
148	06 41 33.49	−50 52 16.3	0.04502640	23.46	23.21	…	…
149	06 41 33.6	−50 53 17.2	0.06592061	23.15	22.84	22.50	…
150	06 41 33.68	−51 02 22.5	0.0607464	23.27	22.95	22.64	…
151	06 41 33.87	−50 57 52.6	0.05790728	23.09	22.83	22.43	…
152	06 41 34.1	−51 04 52.1	0.05515096	23.48	23.13	22.65	…
153	06 41 34.39	−50 59 44.7	0.08287027	22.66	22.33	21.90	…
154	06 41 34.74	−50 52 58.7	0.05223474	23.53	23.24	…	…
155	06 41 35.37	−51 07 57.2	0.05196965	23.55	23.25	…	…
156	06 41 35.62	−50 52 21.0	0.05518927	23.46	23.17	22.75	…
157	06 41 36.08	−51 00 31.2	0.06138969	23.57	23.26	22.64	…
159	06 41 36.81	−50 58 30.4	0.06345606	22.93	22.63	22.10	…
160	06 41 36.91	−51 05 46.8	0.794001	22.95	22.64	17.16	…
161	06 41 37.15	−51 07 26.0	0.06743787	23.32	22.98	22.26	…
162	06 41 37.44	−50 57 44.1	0.04950919	23.44	23.16	…	…
163	06 41 37.52	−50 55 54.8	0.05993709	23.45	23.14	22.58	…
164	06 41 37.61	−50 59 41.7	0.06221228	23.13	22.88	22.04	…
165	06 41 37.68	−50 55 46.8	0.05804816	23.26	23.00	22.46	…
166	06 41 37.77	−50 59 30.2	0.06451736	23.14	22.87	22.49	…
167	06 41 38.48	−50 57 7.7	0.0538934	23.33	23.04	22.46	…
168	06 41 38.71	−51 04 52.4	0.05157579	23.48	23.19	…	…
169	06 41 39.09	−50 50 52.8	0.0494872	23.37	23.12	…	…
170	06 41 39.15	−51 10 26.1	0.05545547	23.46	23.17	…	…
171	06 41 39.34	−50 53 0.5	0.05387548	23.17	22.88	22.54	…
172	06 41 39.47	−50 58 48.9	0.07324209	22.99	22.66	22.19	…
173	06 41 39.55	−50 47 43.3	0.05155752	23.36	23.03	…	…
174	06 41 40.39	−50 54 39.7	0.06174584	23.42	23.12	…	…
175	06 41 40.54	−51 00 58.8	0.05422135	23.43	23.18	…	…
176	06 41 40.59	−50 59 11.0	0.05880960	23.50	23.22	…	…
177	06 41 40.66	−50 46 33.7	0.05548850	23.36	23.03	…	…
178	06 41 41.01	−50 48 45.8	0.05676424	23.42	23.16	…	…
179	06 41 41.45	−51 03 55.3	0.05777849	23.31	22.98	22.50	…
181	06 41 41.67	−50 55 50.3	0.05891665	23.40	23.07	22.53	…
182	06 41 42.16	−51 03 50.8	0.06129068	23.43	23.12	22.69	…
183	06 41 42.21	−50 57 12.3	0.10774755	22.40	22.00	21.51	…
184	06 41 43.02	−51 02 27.1	0.05879365	22.89	22.59	22.17	…
185	06 41 43.11	−51 01 8.2	0.04519765	23.02	22.82	22.59	…
186	06 41 43.19	−51 04 46.4	0.06336417	23.00	22.69	22.27	…
187	06 41 43.51	−51 04 12.0	0.05053246	23.45	23.18	22.75	…
188	06 41 43.56	−50 52 46.5	0.06248493	23.08	22.77	22.30	…
189	06 41 44.16	−51 04 24.9	0.06737899	23.19	22.90	22.50	…
190	06 41 44.58	−51 03 16.4	0.05927821	22.93	22.65	22.24	…
191	06 41 44.66	−51 09 12.9	0.05014270	23.43	23.15	…	…
192	06 41 44.69	−51 02 44.2	0.05215024	23.23	22.95	22.51	…
193	06 41 44.72	−50 50 13.0	0.06786510	23.29	22.99	22.62	…
194	06 41 44.96	−50 54 5.7	0.0638021	23.25	22.94	22.52	…
195	06 41 45.1	−50 56 11.4	0.0604508	23.28	23.00	22.45	…
196	06 41 45.53	−51 01 35.4	0.05485589	23.39	23.11	22.66	…
197	06 41 45.64	−51 05 21.8	0.05700529	23.46	23.19	22.58	…
198	06 41 46.01	−51 04 22.6	0.0552781	23.37	23.14	22.65	…
199	06 41 46.0	−50 53 0.7	0.05127621	23.47	23.15	22.72	…
200	06 41 46.11	−50 50 8.1	0.05729547	22.78	22.20	21.40	…
201	06 41 46.16	−51 12 35.1	0.05264742	23.01	22.76	22.41	…
202	06 41 46.47	−50 55 10.8	0.06236390	23.18	22.92	22.52	V20
203	06 41 46.62	−50 52 43.8	0.05846323	23.16	22.94	22.64	…

Table 13
(Continued)

ID	α	δ	Period (day)	$\langle B\rangle^b$	$\langle V\rangle^b$	$\langle I\rangle^b$	M98
204	06 41 46.72	−50 58 27.3	0.05327753	23.47	23.22	…	…
205	06 41 46.83	−51 05 2.3	0.05975768	23.37	23.04	22.65	…
206	06 41 46.94	−50 58 52.0	0.05747476	23.42	23.15	22.46	…
207	06 41 47.16	−50 53 30.2	0.06124722	22.89	22.59	22.09	…
208	06 41 47.17	−50 59 8.2	0.05641026	22.63	22.37	21.94	…
209	06 41 47.38	−50 51 27.5	0.05379832	23.34	23.05	22.62	…
210	06 41 47.4	−50 49 31.8	0.06601826	23.22	22.95	22.67	…
211	06 41 47.49	−50 54 47.0	0.03863078	23.40	23.09	22.65	…
212	06 41 47.55	−51 00 48.9	0.05764756	23.32	23.04	22.58	…
213	06 41 47.69	−50 54 9.8	0.06027106	23.43	23.12	22.65	…
214	06 41 47.72	−50 52 3.6	0.04701230	23.48	23.22	22.78	…
215	06 41 47.8	−51 01 36.8	0.05662963	23.36	23.10	22.81	…
216	06 41 48.37	−50 50 55.6	0.05979195	23.32	23.03	22.61	…
217	06 41 49.31	−50 57 57.6	0.05807511	23.48	23.16	22.59	…
218	06 41 49.96	−50 46 5.0	0.06366226	23.17	22.94	22.58	…
219	06 41 50.43	−51 04 14.3	0.06075013	23.34	23.08	22.60	…
220	06 41 50.66	−51 00 49.5	0.05904003	23.21	22.90	22.51	…
221	06 41 50.79	−50 58 53.0	0.05209704	23.37	23.08	22.65	…
222	06 41 51.04	−50 54 29.0	0.05576081	23.41	23.11	22.66	…
223	06 41 51.06	−-51 04 31.7	0.06984379	23.21	22.91	22.38	…
224	06 41 51.68	−50 57 27.0	0.05308256	23.38	23.07	22.61	…
225	06 41 51.7	−50 57 4.3	0.07427555	23.23	22.89	22.46	…
226	06 41 51.89	−51 04 1.4	0.05877806	22.95	22.68	22.24	…
227	06 41 51.94	−51 02 46.5	0.04577285	23.06	22.85	22.56	…
228	06 41 52.29	−50 58 7.4	0.05670511	23.31	23.10	22.67	…
229	06 41 52.74	−50 56 50.2	0.05704030	23.32	22.98	22.56	…
230	06 41 52.78	−50 59 12.5	0.05804334	23.58	23.28	…	…
231	06 41 52.83	−51 04 8.9	0.06504728	23.24	22.96	22.56	…
232	06 41 53.2	−50 46 30.9	0.06587775	23.34	23.01	22.59	…
233	06 41 53.2	−50 55 15.6	0.05519357	22.88	22.55	22.08	…
234	06 41 53.3	−51 00 22.5	0.07879928	23.04	22.76	22.34	…
235	06 41 54.04	−50 54 35.2	0.05946258	23.44	23.13	22.60	…
236	06 41 54.11	−51 06 11.7	0.05388561	23.38	23.08	22.61	…
237	06 41 54.81	−51 02 44.2	0.06376287	23.33	23.01	22.57	…
238	06 41 55.75	−50 58 28.9	0.05211579	23.42	23.18	…	…
239	06 41 56.05	−50 48 21.0	0.05420404	23.49	23.23	22.69	…
240	06 41 56.9	−50 58 7.1	0.06098996	23.24	22.96	22.47	…
241	06 41 56.93	−51 06 10.7	0.06707216	23.29	22.97	22.49	…
242	06 41 57.13	−50 56 11.8	0.05633799	22.82	22.52	22.11	V18
243	06 41 57.35	−50 53 3.3	0.05820235	23.45	23.14	22.69	…
244	06 41 57.71	−50 54 22.9	0.03887685	23.28	22.98	22.63	…
245	06 41 58.42	−51 05 46.3	0.06735249	23.27	22.96	22.50	…
246	06 41 58.93	−51 01 35.5	0.06902505	23.13	22.82	22.33	…
247	06 41 59.06	−50 56 14.1	0.07260680	23.19	22.89	22.44	…
248	06 41 59.51	−50 49 7.0	0.05233172	23.48	23.18	…	…
249	06 41 59.69	−50 45 23.6	0.07625333	23.09	22.79	22.32	…
250	06 42 0.03	−50 56 43.3	0.07485741	23.16	22.83	22.44	…
251	06 42 0.05	−50 55 52.2	0.06031459	23.16	22.90	22.57	V17
252	06 42 0.42	−50 57 28.4	0.05574277	23.21	22.96	…	…
253	06 42 0.61	−51 01 38.8	0.05781329	23.53	23.23	22.78	…
254	06 42 0.97	−50 46 12.8	0.07540239	22.73	22.42	22.00	…
255	06 42 0.97	−51 05 20.9	0.05291626	23.51	23.19	…	…
256	06 42 1.11	−50 53 31.3	0.05283800	23.51	23.21	22.74	…
257	06 42 1.31	−51 01 24.7	0.05176433	23.46	23.19	22.72	…
258	06 42 1.72	−51 01 22.7	0.05421737	23.26	23.01	22.57	…
259	06 42 1.83	−50 51 52.9	0.06569699	23.26	22.96	22.53	…
260	06 42 1.88	−50 55 51.3	0.05638275	22.98	22.68	22.28	…
261	06 42 1.97	−50 49 46.9	0.05943899	23.30	23.02	22.65	…
262	06 42 2.65	−50 58 7.1	0.05790880	23.17	22.92	22.38	…
263	06 42 3.21	−50 53 4.3	0.06510705	23.36	23.01	22.54	…
265	06 42 3.72	−50 53 40.1	0.06100386	23.34	23.04	22.59	…
266	06 42 3.84	−50 52 55.2	0.05297954	23.39	23.11	22.62	…
267	06 42 4.06	−50 55 43.7	0.05502621	23.42	23.11	22.69	…
268	06 42 4.51	−50 55 0.6	0.05722660	22.88	22.59	22.19	…

Table 13
(Continued)

ID	α	δ	Period (day)	$\langle B\rangle^b$	$\langle V\rangle^b$	$\langle I\rangle^b$	M98
269	06 42 4.95	−51 05 9.3	0.06504377	23.44	23.12	22.63	…
270	06 42 5.03	−50 58 50.3	0.05499679	23.53	23.23	22.72	…
271	06 42 5.26	−50 55 57.4	0.06152380	23.18	22.86	22.39	…
272	06 42 5.28	−50 49 2.3	0.05880554	23.36	23.07	22.59	…
273	06 42 5.55	−51 02 57.8	0.05339638	23.43	23.15	22.68	…
274	06 42 5.61	−50 55 13.2	0.04986932	23.47	23.20	22.73	…
275	06 42 5.87	−51 01 40.2	0.05530886	23.29	23.03	22.60	…
276	06 42 6.14	−50 56 33.9	0.05151944	23.25	22.95	22.52	…
277	06 42 6.21	−50 57 31.3	0.05929224	23.47	23.14	22.28	…
278	06 42 6.24	−50 46 9.9	0.05903120	23.20	22.91	22.48	…
279	06 42 7.06	−50 59 13.3	0.0689945	23.20	22.91	22.50	…
280	06 42 7.26	−51 03 46.8	0.05790894	22.71	22.50	22.14	…
281	06 42 7.44	−50 56 20.0	0.05449367	22.73	22.44	22.08	…
282	06 42 7.78	−51 12 15.5	0.0677668	23.10	22.79	22.41	…
283	06 42 8.17	−51 06 2.3	0.06326881	22.71	22.40	22.04	…
285	06 42 8.95	−50 49 49.7	0.05939892	23.39	23.10	22.63	…
286	06 42 9.02	−50 47 9.5	0.06478860	23.17	22.91	22.49	…
287	06 42 9.79	−50 53 28.6	0.05328744	23.40	23.12	22.71	…
288	06 42 10.25	−50 45 42.3	0.06449873	23.12	22.89	22.54	…
289	06 42 11.36	−51 03 34.1	0.06686331	23.19	22.92	22.52	…
290	06 42 11.54	−50 51 52.4	0.05631450	23.51	23.22	22.74	…
291	06 42 11.78	−50 56 14.7	0.06001563	23.42	23.10	22.67	…
292	06 42 14.39	−51 01 36.0	0.06529897	23.23	22.94	22.55	…
293	06 42 14.53	−50 47 19.1	0.05494963	23.39	23.10	22.72	…
294	06 42 14.67	−50 53 6.3	0.0590915	23.44	23.11	22.70	…
296	06 42 15.21	−50 58 39.3	0.05625275	23.31	23.03	22.54	…
297	06 42 15.62	−50 54 5.5	0.06991609	23.10	22.84	22.45	…
298	06 42 16.43	−50 56 0.4	0.07426899	23.17	22.85	22.36	…
299	06 42 16.57	−50 51 37.4	0.05705933	23.45	23.15	22.66	…
300	06 42 17.33	−50 58 28.8	0.05419873	23.28	23.02	22.54	…
301	06 42 19.44	−50 55 29.0	0.05615369	22.22	21.92	21.51	…
302	06 42 19.48	−50 43 16.2	0.05671087	23.36	23.07	22.53	…
303	06 42 19.67	−50 55 20.4	0.06518118	23.25	22.93	22.51	…
304	06 42 21.2	−50 56 2.3	0.05414244	22.58	22.30	21.90	…
305	06 42 21.73	−50 52 15.0	0.05867896	23.16	22.89	22.43	…
306	06 42 23.36	−51 03 23.8	0.05754752	23.41	23.07	22.66	…
307	06 42 23.53	−50 49 2.5	0.04933231	23.32	23.13	22.58	…
308	06 42 25.71	−50 44 37.8	0.05746768	23.19	22.97	22.66	…
309	06 42 26.22	−50 54 41.8	0.05833121	23.34	23.08	22.71	…
310	06 42 30.21	−50 47 40.6	0.06787074	23.12	22.86	22.43	…
311	06 42 30.6	−50 46 30.4	0.05826303	23.25	23.03	22.64	…
312	06 42 31.28	−50 56 12.1	0.07580626	23.19	22.88	22.38	…
313	06 42 31.83	−50 50 52.6	0.08140471	23.04	22.75	22.29	…
314	06 42 33.17	−50 56 37.5	0.05044822	23.47	23.23	22.70	…
315	06 42 34.36	−50 50 10.9	0.05782427	23.46	23.15	22.70	…
316	06 42 34.52	−50 52 56.2	0.05146992	23.19	22.90	22.55	…
317	06 42 39.61	−50 51 12.4	0.05268487	23.33	23.03	22.62	…
318	06 42 40.33	−50 55 6.3	0.05775708	23.50	23.21	22.72	…
319	06 42 40.36	−50 54 56.0	0.05554502	23.18	22.77	22.23	…
320	06 42 41.59	−50 57 42.3	0.06197303	22.93	22.62	22.19	…
321	06 42 43.39	−50 46 50.0	0.06700168	23.15	22.88	22.48	…
322	06 42 44.68	−50 55 24.5	0.04944784	23.42	23.16	22.69	…
323	06 42 45.69	−51 02 22.9	0.06264889	23.34	23.02	22.58	…
324	06 42 46.56	−50 56 22.7	0.05710797	23.27	23.01	22.59	…
325	06 42 46.79	−50 34 23.2	0.05855386	23.55	23.22	…	…
326	06 42 49.08	−50 44 54.3	0.06133020	22.88	22.59	22.17	…
327	06 42 54.51	−50 48 8.1	0.06121390	22.92	22.64	22.27	…
328	06 42 54.6	−50 59 11.1	0.05483696	22.96	22.68	22.26	…
329	06 42 55.87	−50 59 7.1	0.05684852	23.38	23.10	22.58	…
330	06 43 4.94	−50 56 3.9	0.06522519	23.12	22.79	22.33	…
331	06 43 10.89	−51 03 42.2	0.05529448	23.39	23.07	22.67	…
332	06 43 18.68	−50 48 19.4	0.05442560	23.07	22.80	22.42	…
333	06 43 22.28	−50 54 17.1	0.06204207	23.32	23.06	22.52	…
334	06 43 27.85	−50 45 51.3	0.05501861	23.30	23.04	22.63	…

Table 13
(Continued)

ID	α	δ	Period (day)	$\langle B\rangle^b$	$\langle V\rangle^b$	$\langle I\rangle^b$	M98
335	06 43 38.45	−50 58 11.4	0.06575684	23.38	23.02	...	...
336	06 43 40.55	−51 02 28.6	0.05646906	23.45	23.18	...	...
337	06 43 51.08	−50 50 27.7	0.05884652	23.46	23.16	...	...
338	06 44 43.03	−50 47 50.2	0.05083201	23.42	23.19	...	...
...	06 41 02.39	−51 01 53.3	0.06397398	23.32	23.02	22.54	V1
...	06 41 09.57	−51 01 20.6	0.04791289	23.46	23.15	22.73	V2
...	06 41 04.12	−51 01 14.7	0.07691745	23.19	22.88	22.40	V3
...	06 40 57.75	−51 00 11.4	0.06608899	23.11	22.83	22.40	V6
...	06 41 02.86	−50 59 40.4	0.05093715	23.42	23.13	22.74	V7
...	06 40 56.40	−50 59 39.8	0.05575196	23.50	23.14	22.79	V8
...	06 41 02.22	−50 58 54.7	0.07171579	23.09	22.77	22.36	V11
...	06 41 56.74	−50 56 13.7	0.05907561	23.08	22.78	22.35	V18
...	06 41 55.20	−50 56 15.4	0.06491275	22.86	22.58	22.17	V19

Monelli was supported by the Education and Science Ministry of Spain (grants AYA2010-16717). M. Fabrizio acknowledges financial support from the PO FSE Abruzzo 2007-2013 through the grant "Spectro-photometric characterization of stellar populations in Local Group dwarf galaxies, prot.89/2014/OACTe/D (PI: S. Cassisi). G. Fiorentino was supported by the Futuro in Ricerca 2013 (RBFR13J716).

APPENDIX
NOTES ON INDIVIDUAL VARIABLES

V11, V26, V74: Classified as first-overtone pulsators by S86, according to the current photometry they seem to be double-mode pulsators.

V17: Classified as a suspected variable in S86 and NV by D03. According to the current photometry it appears to be an EB with a period of 0.3933393 days.

V22: Classified as first-overtone pulsator by S86 and D03. According to the current photometry it seems to pulsate in the fundamental mode with period of days.

V25, V31: Classified as first-overtone pulsators by S86. According to the current photometry they seem to pulsate in the fundamental mode with periods of 0.05765942 and 0.06037914 days and they also show the Blazhko effect.

V27, V29, V33, V129 and V149: Classified as fundamental mode pulsators by S86. According to the current photometry they appear to be ACs.

V40 and V115: Classified as uncertain variables by S86. According to our current set of data, they appear to pulsate as first-overtones and ACs, respectively.

V41 and V87: Classified as suspected variables by S86. According to our current set of data, they appear to be anomalous cepheids.

V61, V77, V126, V127: Classified as fundamental mode pulsators by S86. According to the current photometry they also show the Blazhko effect.

V89: Classified as a fundamental mode pulsator by S86. According to the current photometry it seems to be a double-mode pulsator.

V138 and V141: Classified as suspected variables by S86. According to our current set of data, they appear to be fundamental-mode pulsators.

V142 and V151: Classified as suspected variables by S86. According to our current set of data, they appear to be first overtone pulsators.

V176: Classified as a first-overtone pulsator by D03 with period of ∼0.4. According to the current photometry it seems to pulsate in the fundamental mode with period of 0.764565 days.

V40, V65, V73, V84, V85, V123, V136, V138, V149, V177, V183, V186, V188, V195, V199, V201, V208, V211, V227, V228, V229, V230: The *I*-band light curves are poorly sampled in the pulsation across maximum light.

V31, V61, V76, V77, V126, V127, V206: Classified as fundamental pulsators by D03. According to the current photometry they seem to pulsate in the fundamental mode and they also show the Blazhko effect.

V74: Classified as a first overtone pulsator by D03. According to the current photometry they seem to pulsate in the double mode.

V85, V90, V181, V186, V196, V226: The light curves are noisy.

V148: This RR_c is ∼0.3 mag brighter than the typical luminosity of HB stars.

V158, V182: We confirm the peculiar nature of the RRLs (see also Paper VI).

V161: Classified as a suspected variable in D03. According to the current photometry it does not show variability.

V170 and V171: Not enough data to fit light curves; uncertain parameters.

V176, V179, V196, V182, V200, V223: These RRLs have very small luminosity amplitudes for an ab-type RRL.

V181: This variable has a very small luminosity amplitude for a c-type RRL. Possible blend with nearby faint star.

V193, V205, V216 , V217, V219: These variables have very small amplitudes for an AC-type variable. Possible blends with nearby faint stars.

V3, V25, V44, V58, and V133: These stars were classified as newly discovered variables in Paper VI with the identification numbers: V215, V213, V212, V211, and V209, respectively.

V4, V32, V41 and V165: These stars were classified in D03 and Paper VI as V177, V202, V180 and V165, respectively.

V218, V227, V228, V229, V230: Poorly sampled light curves, pulsational parameters are uncertain.

RRL-1, RRL-2, RRL-3, RRL-4, RRL-5, RRL-38, AC-1, AC-9, AC-10: These stars are the six RRLs (three RR_c, three RR_{ab}) and the three ACs recently detected by VM13 outside the tidal radius of Carina.

REFERENCES

Baldry, I. K., Driver, S. P., Loveday, J., et al. 2012, MNRAS, 421, 621
Bauer, A. E., Conselice, C. J., Pérez-González, P. G., et al. 2011, MNRAS, 417, 289
Benedict, G. F., McArthur, B. E., Feast, M. W., et al. 2011, AJ, 142, 187
Bessell, M. S. 1969, ApJS, 18, 195
Blanco-Cuaresma, S., Soubiran, C., Heiter, U., et al. 2015, A&A, 577, A47
Bono, G., Caputo, F., Cassisi, S., Incerpi, R., & Marconi, M. 1997a, ApJ, 483, 811
Bono, G., Caputo, F., Castellani, V., & Marconi, M. 1997b, A&AS, 121, 327
Bono, G., Caputo, F., & di Criscienzo, M. 2007, A&A, 476, 779
Bono, G., Caputo, F., & Marconi, M. 1995, AJ, 110, 2365
Bono, G., Dall'Ora, M., Caputo, F., et al. 2011, in RR Lyrae Stars, Metal-Poor Stars, and the Galaxy, ed. A. McWilliam (Pasadena, CA: The Carnegie Institution), 1
Bono, G., Marconi, M., Cassisi, S., et al. 2005, ApJ, 621, 966
Bono, G., Stetson, P. B., Walker, A. R., et al. 2010, PASP, 122, 651
Braga, V. F., Dall'Ora, M., Bono, G., et al. 2015, ApJ, 799, 165
Bragaglia, A., Gratton, R. G., Carretta, E., et al. 2001, AJ, 122, 207
Cacciari, C., Corwin, T. M., & Carney, B. W. 2005, AJ, 129, 267
Caputo, F. 1998, A&ARv, 9, 33
Cardelli, J. A., Clayton, G. C., & Mathis, J. S. 1989, ApJ, 345, 245
Carretta, E., Bragaglia, A., Gratton, R., D'Orazi, V., & Lucatello, S. 2009, A&A, 508, 695
Carretta, E., Bragaglia, A., Gratton, R. G., et al. 2010, A&A, 520, AA95
Castellani, V., Chieffi, A., & Pulone, L. 1991, ApJS, 76, 911
Castellani, V., & degl'Innocenti, S. 1995, A&A, 298, 827
Clement, C. M., Ferance, S., & Simon, N. R. 1993, ApJ, 412, 183
Clement, C. M., Kinman, T. D., & Suntzeff, N. B. 1991, ApJ, 372, 273
Clement, C. M., & Shelton, I. 1999, ApJL, 515, L85
Clementini, G., Cignoni, M., Contreras Ramos, R., et al. 2012, ApJ, 756, 108
Clementini, G., Corwin, T. M., Carney, B. W., & Sumerel, A. N. 2004, AJ, 127, 938
Clementini, G., Di Tomaso, S., di Fabrizio, L., et al. 2000, AJ, 120, 2054
Cole, A. A., Skillman, E. D., Tolstoy, E., et al. 2007, ApJL, 659, L17
Coppola, G., Stetson, P. B., Marconi, M., et al. 2013, ApJ, 775, 6 (Paper VI)
Cox, A. N., Hodson, S. W., & Clancy, S. P. 1983, ApJ, 266, 94
Cseresnjes, P. 2001, A&A, 375, 909
Da Costa, G. S., & Hatzidimitriou, D. 1998, AJ, 115, 1934
Dalessandro, E., Ferraro, F. R., Massari, D., et al. 2013, ApJ, 778, 135
Dall'Ora, M., Clementini, G., Kinemuchi, K., et al. 2006, ApJL, 653, L109
Dall'Ora, M., Kinemuchi, K., Ripepi, V., et al. 2012, ApJ, 752, 42
Dall'Ora, M., Ripepi, V., Caputo, F., et al. 2003, AJ, 126, 197 (D03)
Di Criscienzo, M., Greco, C., Ripepi, V., et al. 2011, AJ, 141, 81
Di Criscienzo, M., Marconi, M., & Caputo, F. 2004, ApJ, 612, 1092
Drake, A. J., Djorgovski, S. G., Mahabal, A., et al. 2009, ApJ, 696, 870
Duncan, K., Conselice, C. J., Mortlock, A., et al. 2014, MNRAS, 444, 2960
Eggen, O. J. 1979, ApJS, 41, 413
Eyer, L., Palaversa, L., Mowlavi, N., et al. 2012, Ap&SS, 341, 207
Fabrizio, M., Nonino, M., Bono, G., et al. 2015, arXiv:1505.06597
Fabrizio, M., Raimondo, G., Brocato, E., et al. 2014, A&A, 570, AA61
Fiorentino, G., Bono, G., Monelli, M., et al. 2015a, ApJL, 798, L12
Fiorentino, G., Bono, G., Monelli, M., et al. 2015b, ApJ, 810, 15
Fiorentino, G., Lanzoni, B., Dalessandro, E., et al. 2014, ApJ, 783, 34
Fiorentino, G., Limongi, M., Caputo, F., & Marconi, M. 2006, A&A, 460, 155
Fiorentino, G., Musella, I., & Marconi, M. 2013, MNRAS, 434, 2866
Fiorentino, G., Stetson, P. B., Monelli, M., et al. 2012, ApJL, 759, L12
Gallart, C., Zoccali, M., & Aparicio, A. 2005, ARA&A, 43, 387
Garcia-Melendo, E., & Clement, C. M. 1997, AJ, 114, 1190
Garofalo, A., Cusano, F., Clementini, G., et al. 2013, ApJ, 767, 62
Gilliland, R. L., Bono, G., Edmonds, P. D., et al. 1998, ApJ, 507, 818
Gratton, R. G., Bragaglia, A., Clementini, G., et al. 2004, A&A, 421, 937
Greco, C., Dall'Ora, M., Clementini, G., et al. 2008, ApJL, 675, L73
Haschke, R., Grebel, E. K., Frebel, A., et al. 2012, AJ, 144, 88
Hatzidimitriou, D., Papadakis, I., Croke, B. F. W., et al. 1999, AJ, 117, 3059
Hog, E., & Petersen, J. O. 1997, A&A, 323, 827
Kaluzny, J., & Thompson, I. B. 2003, AJ, 125, 2534
Kirby, E. N., Cohen, J. G., Guhathakurta, P., et al. 2013, ApJ, 779, 102
Kovács, G. 2001, A&A, 375, 469
Kuehn, C., Kinemuchi, K., Ripepi, V., et al. 2008, ApJL, 674, L81
Kunder, A., & Chaboyer, B. 2008, AJ, 136, 2441
Kunder, A., Stetson, P. B., Cassisi, S., et al. 2013, AJ, 146, 119
Layden, A. C. 1994, AJ, 108, 1016
Madore, B. F. 1982, ApJ, 253, 575
Madore, B. F., Hoffman, D., Freedman, W. L., et al. 2013, ApJ, 776, 135
Marconi, M., Bono, G., Caputo, F., et al. 2011, ApJ, 738, 111
Marconi, M., Coppola, G., Bono, G., Braga, V., et al. 2015, ApJ, 808, 50
Marconi, M., Fiorentino, G., & Caputo, F. 2004, A&A, 417, 1101
Marconi, M., Ripepi, V., Alcalá, J. M., et al. 2000, A&A, 355, L35
Marengo, M., Evans, N. R., Barmby, P., et al. 2010, ApJ, 709, 120
Mateo, M., Hurley-Keller, D., & Nemec, J. 1998, AJ, 115, 1856
Matsunaga, N., Feast, M. W., Kawadu, T., et al. 2013, MNRAS, 429, 385
Matsunaga, N., Kawadu, T., Nishiyama, S., et al. 2011, Natur, 477, 188
McConnachie, A. W. 2012, AJ, 144, 4
McNamara, D. H. 1995, AJ, 109, 1751
McNamara, D. H. 2000, PASP, 112, 1096
McNamara, D. H. 2011, AJ, 142, 110
McNamara, D. H., & Barnes, J. 2014, AJ, 147, 31
Miceli, A., Rest, A., Stubbs, C. W., et al. 2008, ApJ, 678, 865
Monelli, M., Bernard, E. J., Gallart, C., et al. 2012a, MNRAS, 422, 89
Monelli, M., Cassisi, S., Mapelli, M., et al. 2012b, ApJ, 744, 157
Monelli, M., Gallart, C., Hidalgo, S. L., et al. 2010a, ApJ, 722, 1864
Monelli, M., Hidalgo, S. L., Stetson, P. B., et al. 2010b, ApJ, 720, 1225
Monelli, M., Milone, A. P., Fabrizio, M., et al. 2014, ApJ, 796, 90
Monelli, M., Pulone, L., Corsi, C. E., et al. 2003, AJ, 126, 218
Moretti, M. I., Dall'Ora, M., Ripepi, V., et al. 2009, ApJL, 699, L125
Mortlock, A., Conselice, C. J., Hartley, W. G., et al. 2013, MNRAS, 433, 1185
Musella, I., Ripepi, V., Clementini, G., et al. 2009, ApJL, 695, L83
Musella, I., Ripepi, V., Marconi, M., et al. 2012, ApJ, 756, 121
Nemec, J., & Mateo, M. 1990, in ASP Conf. Ser. 10, Evolution of the Universe of Galaxies, Vol. 10, ed. R. G. Kron (San Francisco, CA: ASP), 134
Nemec, J. M. 1985a, AJ, 90, 204
Nemec, J. M. 1985b, AJ, 90, 240
Niss, B. 1981, A&A, 98, 415
Okamoto, S., Arimoto, N., Yamada, Y., & Onodera, M. 2008, A&A, 487, 103
Olech, A., Dziembowski, W. A., Pamyatnykh, A. A., et al. 2005, MNRAS, 363, 40
Palaversa, L., Ivezić, Ž, Eyer, L., et al. 2013, AJ, 146, 101
Petersen, J. O. 1991, A&A, 243, 426
Petersen, J. O., & Christensen-Dalsgaard, J. 1999, A&A, 352, 547
Pietrinferni, A., Cassisi, S., Salaris, M., & Castelli, F. 2004, ApJ, 612, 168
Pietrzyński, G., Górski, M., Gieren, W., et al. 2009, AJ, 138, 459
Pojmanski, G. 2002, ACTAA, 52, 397
Romaniello, M., Primas, F., Mottini, M., et al. 2008, A&A, 488, 731
Saha, A., Monet, D. G., & Seitzer, P. 1986, AJ, 92, 302
Salvadori, S., Ferrara, A., Schneider, R., Scannapieco, E., & Kawata, D. 2010, MNRAS, 401, L5
Sandage, A., Katem, B., & Sandage, M. 1981, ApJS, 46, 41
Sanna, N., Bono, G., Stetson, P. B., et al. 2009, ApJL, 699, L84
Santolamazza, P., Marconi, M., Bono, G., et al. 2001, ApJ, 554, 1124
Smith, H. A. 2006, MmSAI, 77, 492
Soszyński, I., Dziembowski, W. A., Udalski, A., et al. 2011, ACTAA, 61, 1
Soszynski, I., Poleski, R., Udalski, A., et al. 2008, ACTAA, 58, 163
Soszyñski, I., Udalski, A., Szymañski, M. K., et al. 2009, ACTAA, 59, 1
Soszyñski, I., Udalski, A., Szymañski, M. K., et al. 2010, ACTAA, 60, 165
Soszyñski, I., Udalski, A., Szymañski, M. K., et al. 2014, ACTAA, 64, 177
Springel, V., White, S. D. M., Jenkins, A., et al. 2005, Natur, 435, 629
Stetson, P. B., Braga, V. F., Dall'Ora, M., et al. 2014a, PASP, 126, 521
Stetson, P. B., Fiorentino, G., Bono, G., et al. 2014b, PASP, 126, 616
van Albada, T. S., & Baker, N. 1971, ApJ, 169, 311
van den Bergh, S. 1975, in Galaxies and the Universe, ed. A. Sandage, M. Sandage, & J. Kristian (Chicago, IL: Univ. of Chicago Press), 509
Vivas, A. K., & Mateo, M. 2013, AJ, 146, 141 (VM13)
Vivas, A. K., Zinn, R., Abad, C., et al. 2004, AJ, 127, 1158
Walker, A. R. 1994, AJ, 108, 555
Walker, A. R., & Nemec, J. M. 1996, AJ, 112, 2026
Walker, A. R., & Terndrup, D. M. 1991, ApJ, 378, 119
Weinzirl, T., Jogee, S., Conselice, C. J., et al. 2011, ApJ, 743, 87
Zinn, R., & West, M. J. 1984, ApJS, 55, 45
Zoccali, M., Hill, V., Lecureur, A., et al. 2008, A&A, 486, 177